Alma Mater Studiorum – Università di Bologna

DOTTORATO DI RICERCA IN NEUROFISIOLOGIA
XXI Ciclo

Settore scientifico disciplinare di afferenza:
BIO/09 FISIOLOGIA

Role of BDNF secretion and signaling in the activity-dependent refinement of synaptic connections

Dott. Matteo Bergami

Coordinatore Dottorato:
Prof. Claudio Galletti

Relatore:
Prof. Giorgio Aicardi

Esame finale anno 2009

INDEX

INTRODUCTION

1 BDNF as modulator of synaptic functions

1.1 The neurotrophins and their receptors

Neurotrophins (NTs) are a family of trophic factors that include nerve growth factor (NGF), brain-derived neurotrophic factor (BDNF), neurotrophin-3, and neurotrophin-4/5 (NT-3, NT-4/5) (Thoenen, 1995; Poo, 2001). NTs bind two structurally unrelated types of membrane receptor, a high affinity tyrosine receptor kinase (Trk) and a low-affinity pan-neurotrophin receptor ($p75^{NTR}$). Each Trk is preferentially activated by one or more NTs (TrkA by NGF, TrkB by BDNF and NT-4/5, and TrkC by NT-3) whereas $p75^{NTR}$ binds all NTs with similar nanomolar affinities (Fig. 1). Although NTs bind as dimers to both Trk and $p75^{NTR}$, these receptors show indipendent signalling properties. The binding of NTs to Trk receptors induces their dimerization and autophosphorylation of tyrosine residues located in the intracellular domain; in turn, this mechanism promotes the activation of intracellular signaling cascades, comprising the Shc (Src homologous and collagen-like) and PLC-γ (phospholipase C-γ) pathways (Fig. 2), responsible for inducing transcriptional events modulating different cellular aspects such as cell cycle, cell survival, neurite outgrowth and synaptic transmission (Chao, 2003). Through a different set of adaptor proteins, $p75^{NTR}$ can act on the effectors JNK (Jun N-terminal kinase), NF-κB and ceramide, which are involved in inducing apoptosis of neurons (Chao, 2003).

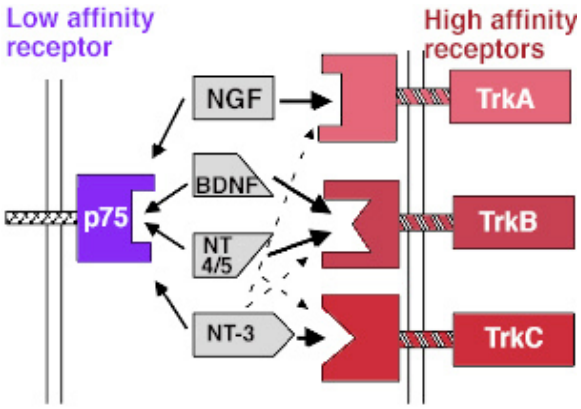

Figure 1. **Each Trk receptor is preferentially activated by one or more NTs whereas $p75^{NTR}$ binds all NTs with similar nanomolar affinities.**

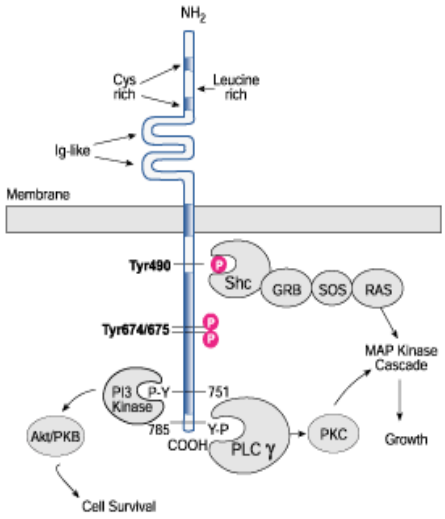

Figure 2. **Schematic structure of Trk receptors: upon activation, phosphorilated tyrosine residues in the intracellular domain promote signaling pathways which influence cell growth, survival, neurite outgrowth and synaptic ttransmission.**

1.2 Regulation of BDNF synaptic trafficking

In addition to their classical trophic role, NTs, in particular BDNF, are thought to participate in certain brain functions such as modulation of synaptic transmission and memory formation (Lu 2004; Poo 2001; Thoenen, H., 2000). The physiological relevance of this action is based on the observation that BDNF differentially modulates activity-dependent changes in synaptic strength, as reflected by long-term potentiation (LTP) and long-term depression (LTD), which are cellular paradigms for learning and memory (McAllister et al, 1999; Thoenen, 2000; Poo, 2001; Lu, 2004). In order to initiate and maintain the LTP response, BDNF must be available at concentrations that reach a critical threshold level. This phenomenon has been demonstrated in heterozygous BDNF-defective mice that, having impaired endogenous NT production, require either the exogenous administration or local re-expression of BDNF to initiate the LTP response (Korte et al, 1995, 1996; Patterson et al, 1996). These observations emphasize the need to understand better how BDNF availability could be regulated. Neuronal activity regulates BDNF availability at three different levels, namely by increasing transcription (Shieh et al, 1998; Chen et al, 2003), translation (Schratt et al, 2004) and secretion (Balkowiec and Katz, 2000; Hartmann et al, 2001; Aicardi et al, 2004). Recent studies have established that all these regulatory events are critical steps in the late, persistent phase of LTP, which is dependent on gene transcription and protein translation (Kandel, 2001). Overexpression of mRNA BDNF transcripts in transgenic mice carrying a constitutively activated form of CREB resulted in a late-phase LTP independent of new transcription in hippocampal CA1 neurons (Barco et al, 2005). Moreover, exogenous BDNF administered to mouse hippocampal slices rescued LTP impaired by protein synthesis inhibition (Pang et al, 2004). Thus, increased BDNF availability can overcome the physiological requirement for BDNF transcription and translation induced by high-frequency stimulation.

For the understanding of the activity-dependent regulation of BDNF availability, it is important to identify the pathways by which it is supplied to the site(s) of secretion. BDNF is synthesized in the soma, packaged into post-Golgi membrane-confined compartments and transported to either dendritic domains or

axon terminals (Poo, 2001). BDNF synthesis has also been observed in dendrites of cultured hippocampal neurons (Tongiorgi et al, 1997). However, BDNF has been detected in neurons that lack BDNF mRNA transcripts (Conner et al, 1997), suggesting that it has been taken up by these cells. Evidence for this process has been provided by studies on transneuronal transfer of NTs in the visual system of chick and rodents. Injection of BDNF or neurotrophin-3 (NT-3) into the eyes of chick embryos (von Bartheld et al, 1996; Butowt and von Bartheld, 2001; Wang et al, 2002) or adult rodents (Caleo et al, 2000, 2003; Butowt and von Bartheld, 2005) led to their uptake by retinal ganglion cells, transport to the axon terminals and secretion, resulting in survival of target neurons (von Bartheld et al, 1996; Caleo et al, 2000, 2003) and synaptic plasticity (Wang et al, 2002). What is the fate of the endocytosed BDNF, and to which extent it contributes to the increased BDNF availability required for synaptic plasticity, still remain questions to be elucidated.

An additional interesting aspect of BDNF trafficking is the possibility that its internalization could be extended to astrocytes, the third cellular component of the synaptic contacts. In this respect, BDNF immunoreactivity has been detected in astrocytes enwrapping the giant boutons along the hippocampal mossy fiber pathway, suggesting that they can internalize it at synaptic sites (Danzer and McNamara, 2004). Astrocytes are known to play an active role in modulating synaptic transmission; they express many of the same receptors as neurons, and this feature makes astrocytes sensitive to secreted neuronal neurotransmitters, to which they respond with a rise in Ca^{2+} ions and the release of various active substances such as ATP, which act back on neurons to influence neuronal activity (Volterra and Meldolesi, 2005). Moreover, atrocytes are responsible for terminating the action of neurotransmitters secreted by neurons and for mediating their recycling back to neurons through the glutamate-glutamine cycle. Considering the modulatory effects of astrocytes to synaptic transmission and the presence of BDNF receptors on their processes, an intriguing hypothesis is that these cells could significantly contribute to the overall availability of this NT in the synaptic cleft. Given the functional implications of BDNF trafficking and availability on synaptic plasticity it is important to clarify these aspects at molecular and functional levels.

1.3 Activity-dependent secretion of BDNF

Activity-dependent secretion of BDNF has been largely demonstrated to be required for the expression and maintenance of LTP of the synaptic transmission (McAllister et al, 1999; Thoenen, 2000; Poo, 2001; Lu, 2004). The canonical NTs secretory pathway anticipates that the synthesized precursors of these proteins undergo an intracellular processing within the trans-Golgi network by proteases before being packaged into vesicles of small diameter (50-100 nm) for their secretion, and then continuously released into the extracellular environment (Lessman et al, 2003; Mowla et al, 1999). However, it has been demonstrated that BDNF release represents an exception to this mechanism, being able to get packaged into large diameter vesicles (~300 nm) and secreted via a regulatory pathway that is critically dependent of intracellular Ca^{2+} and controlled by neuronal activity (Balkowiec and Katz 2000; Lever et al, 2001; Canossa et al, 2001; Aicardi et al, 2004). It seems now clear that this kind of secretion requires specific sorting motifs which are accessible when BDNF is in its precursor form; both the *mature* and the *pro* domains of *pro*BDNF carry precise amino acid sequences which are responsible for the regulated secretion of this NT. For example, the interaction of one motif in the *mature* domain with the sorting receptor carboxipeptidase E (CPE) directly targets BDNF toward the regulated secretory pathway (Lou et al, 2005); similarly, the interaction of a specific motif in the *pro* domain with the protein sortilin is also required for proper trafficking and targeting of BDNF toward the regulated pathway of secretion (Chen et al. 2004; Egan et al. 2003). Once formed, the BDNF-containing vesicles are then transported into neuronal processes, either axons or dendrites (Kohara et al, 2001; Hartmann et al, 2001), where they are secreted and exert their synaptic functions according to neuronal activity. Until recently, it was commonly accepted that within the secretory granules budding off the trans-Golgi network a complete processing of *pro*BDNF would occur, leading to the final release of mature BDNF from the neurons. As mentioned, this process requires the cleavage of the *pro* domain from the *mature* part of the protein, a task which can be performed by furin or pro-protein convertases located in the granules themselves (Lessman et al, 2003). However, a

series of recent studies suggest that, upon neuronal activation, *pro*BDNF can be secreted as such and subsequently cleaved in the extracellular environment by proteases such as plasmin or metalloproteases (Lee et al, 2001; Pang et al, 2004). Supporting this hypothesis is also the finding that BDNF mRNA occurs in two splice variants, one of which is selectively transported to the dendrites of neurons, where local synthesis of the NT together with the lack of the proper machinery for its processing may favor the direct secretion of *pro*BDNF (An et al, 2008). Given the fact that *pro*BDNF preferentially binds and activate $p75^{NTR}$, whereas *mature* BDNF selectively activates TrkB receptors (Chao et al, 2003), the processes governing the proteolisis of proBDNF and therefore controlling the BDNF isoform (*pro* vs. *mature*) that is finally secreted in the synaptic cleft would provide an intriguing mechanism by which BDNF could exert its biological actions. Indeed, in terms of synaptic plasticity, the relative proportion of secreted BDNF isoforms has been suggested to differently influence synaptic transmission, with *pro*BDNF preferentially activating $p75^{NTR}$ to mediate synaptic depression and *mature* BDNF activating TrkB receptors to contribute to synaptic potentiation (Lu, 2005). Given the importance to discriminate if, and to which degree, *pro*BDNF is efficiently secreted from CNS neurons, some groups have recently attempted to quantify the effective proportion of secreted *pro* versus *mature* BDNF (Matsumoto et al, 2008; Yang et al, 2009). Surprisingly, although both groups used a similar neuronal culture system in order to measure the secretion of endogenous *pro*BDNF, they clearly provided opposite results. Whether *pro*BDNF is or not secreted, and to which extent the different synaptic partners contribute to BDNF availability, are therefore still matters of debate, and given the functional implications of these mechanisms in synaptic plasticity they represent key points in the fast synaptic action of NTs which are important to clarify.

1.4 Specific Aims

To improve our understanding on the mechanisms controlling BDNF availability at synaptic sites, we tracked BDNF, either in its *pro* and *mature* form, in (i) dissociated neuronal and/or astrocytic culture and (ii) brain slices

during potentiation of the synaptic transmission. By using electrophysiological approaches and imaging tecniques, we evaluated the trafficking and recycling of *pro*BDNF/*mature* BDNF both in neuronal and astrocitic compartments.

2 Role of BDNF signaling in adult hippocampal neurogenesis

2.1 Adult hippocampal neurogenesis

The lifelong generation of new neurons is well documented in the subgranule zone of the dentate gyrus in the hippocampus (Altman and Das, 1965; Eriksson et al, 1998). Dentate gyrus neurons result from local self replicating radial glia-like stem cells (Doetsch et al, 1999; Seri et al, 2001; Ninkovic et al, 2007). Once generated, the vast majority of neurons remain located on the hilar side of the granule layer (Seri et al, 2004) and attempt to connect into the existing neuronal network, finally receiving afferent input from perforant path fibers (van Praag et al, 2002; Toni et al 2007) and providing efferent output to CA3 cells (Hastings and Gould, 1999; Markakis and Gage, 1999). While new neurons are held to incorporate into the pre-existing circuitry via a stereotypical sequence of morphological transitions, a detailed description of this process has only recently been described in mice using retroviral mediated birthdating analysis (Zhao et al, 2006). Axons and dendrites initiate their growth around 3 days post retroviral injection. While axons enter the CA3 areas of the hippocampus after 10 days, dendrites grow through the outer edge of the molecular layer where they attain a high level of complexity by approximately 8 weeks of age, creating the basic organization of synaptic connections. Integration of adult-born neurons requires prior development of dendritic spines and formation of functional synapses (Toni et al, 2007). Spine growth starts at day 16 after a neuron is born, while spine density is sharply increased only at day 28, slowly reaching the final plateau after 6 weeks (Zhao et al, 2006). However, a substantial population of newly generated neurons fail to integrate and eventually die (Kempermann et al,

2003). Indeed, it has recently been demonstrated that the proportion of adult-born neurons within the hippocampal network is kept at rather constant levels (about 10%) thereby creating a pool of constantly renewed/turned-over neurons versus a stable pool of neurons persisting from developmental/embryonic stages (Ninkovic et al, 2007).

Despite many factors influencing adult neurogenesis (Zhao et al, 2008), the molecular mechanisms regulating the functional integration and/or survival of newborn neurons are not yet fully understood. There is growing evidence of the role of neuronal activity in this process (Ge et al, 2006; Tashiro et al, 2006). New neurons sense neuronal activity through ambient GABA (γ-aminobutyric acid) before receiving, in sequence, GABAergic and glutamatergic inputs. Defects in the GABA responsiveness of newborn neurons, such as that obtained by inducing the conversion of GABA-mediated depolarization into hyperpolarization, lead to marked deficits in dendritic arborisation and synapse formation (Ge et al, 2006), suggesting that network activity controls key morphological transitions required for the connectivity of adult-born neurons. At the initiation of connectivity glutamatergic inputs control newborn neuron survival (Tashiro et al, 2006). Indeed, access to afferent inputs may be the key for their life and death decision. A central hypothesis arising from this regulation is that adult-born neurons could contribute to the formation of new circuits in tune with network needs, which, in turn, relates to the functional incorporation of adult-born neurons into hippocampal circuits. Hence, around connectivity and longer time adult-born neurons become preferentially recruited into functional networks, i.e memory networks (Kee et al, 2007), and selectively express enhanced synaptic plasticity (Ge et al, 2007). As neurogenesis continuously proceeds, the integration of adult-born neurons may play a key role in the anatomical and functional plasticity of hippocampal circuitry, which have been thought to underlie complex cognitive (Aimone et al, 2006; Liedo et al, 2006) and emotional (Sahay and Hen, 2007) functions.

2.2 Influence of BDNF on hippocampal neurogenesis

Neurogenic niches in the mammalian adult brain are thought to share a specialized microenvironment which is permissive for the proliferation of progenitor cells and at the same time promotes the differentiation, maturation and recruitment of their neuronal progeny into the pre-existing circuitry. The signaling mechanisms that influence this microenvironment, and therefore regulate the different steps necessary for the generation of new neurons, have just started to be elucidated. Because of its established roles in the developing nervous system, BDNF quickly emerged as candidate modulator of adult neurogenesis. In the last years, a certain amount of correlative data suggested that BDNF could contribute to the neurogenic milieu by regulating the extent of adult neurogenesis in the SGZ of the hippocampus and the SVZ of the lateral ventricle. Starting from *in vitro* studies of explanted neuronal progenitors (Chiaramello et al, 2007) and direct overexpression or infusion of BDNF or BDNF scavengers (TrkB-IgGs) into the neurogenic areas of the adult brain (Zigova et al, 1998; Benraiss et al, 2001; Pencea et al, 2001; Scharfman et al, 2005), a number of studies strengthen the link between BDNF-TrkB signaling and adult neurogenesis. The common idea arising from these studies identifies in the neurotrophin BDNF a factor capable of sustaining and increasing the generation of new cells. Following works provided further evidences along this line: by the use of transgenic mice bearing half of BDNF protein (Rossi et al, 2006; Sairanen et al, 2005) or a mutated isoform of the TrkB receptor (Sairanen et al, 2005), the survival of newborn neurons resulted affected, suggesting the requirement of this neurotrophin for the process of neurogenesis. Despite all these reports, many questions remain about how BDNF actually affects neurogenesis. It is unclear, for example, whether the neurogenic action of BDNF is due primarily to effects on rate of cell division versus survival and differentiation of newborn cells. A critical step in addressing these questions is to first understand at which stages BDNF might act to modulate development of neural precursors in the adult hippocampus and whether its actions influence cell fate specification and terminal differentiation of these cells in vivo. Besides these characterizations, the process of integration of new neurons in an already established network suggests the capacity of these new elements to influence, and get influenced by, the overall activity. BDNF represent a key mediator in the

regulation of developing and mature synaptic functions, in particular because it is expressed and secreted at the synapses in an activity-dependent fashion; therefore, BDNF appears a good candidate for regulating the process of maturation and integration of new neurons according to hippocampal network's activity.

2.3 Specific Aims

To work out the role of BDNF in adult hippocampal neurogenesis, we investigated the effects of BDNF signaling on newborn neurons integration in the pre-existing network at the time of formation of new synaptic connections. To this aim, transgenic mouse models, virus technology and confocal microscopy were used as techniques to study the influence of BDNF signaling in the process of maturation of new neurons *in vivo*. The impact of their integration in the hippocampal network was evaluated by electrophysiological recordings and behavioral analysis.

RESULTS

1. Neuron-neuron and neuron-glia trancytosis of BDNF during synaptic potentiation

1.1 Activity-dependent *pro*BDNF secretion and transfer to perineuronal astrocytes

To investigate the pattern of BDNF expression and secretion in rensponse to LTP induction, field recordings were performed in layers II/III of rat perirhinal cortex slices (Fig. 1*A*) subjected to either basal (0.033 Hz) or TBS (100 Hz) stimulation. BDNF secretion was measured in the collected perfusion medium by ELISA (Fig. 1*C*). Although BDNF levels remained constant during basal stimulation, TBS induced a rapid, transient increase in BDNF in the perfusate, which correlated with induction of synaptic potentiation of the field potential as previously described (Aicardi et al., 2004). BDNF expression in slices was examined by immunostaining; Fig. 1*C* shows representative examples of *pro*BDNF immunoreactivity in the perirhinal cortex upon basal and TBS stimulation using an antibody directed specifically against the *pro* region of the neurotrophin (Fig. 1*B*). Basal levels of *pro*BDNF immunoreactivity were detected proximal to (Fig. 1*A*, region A1) and distal from (Fig. 1*A*, region A2) the stimulation electrode in controls. A marked increase in *pro*BDNF immunoreactivity was observed after TBS, which gradually declined distally from the stimulation electrode. This effect was blocked by prior treatment with the protein synthesis inhibitor anisomycin, consistent with the *pro*BDNF increase depending on activity-dependent local protein synthesis (Kandel, 2001). Similar results were obtained using an antibody directed against the *mature* portion of the neurotrophin that recognizes both *mature* and *pro*BDNF (Fig. 1*D*). High resolution confocal analysis of individual neurons in the A1 region confirmed that *pro*BDNF immunoreactivity was increased after TBS (Fig. 1*E* and Fig. 2*A*). Surprisingly, *pro*BDNF was also localized in perineuronal astrocytes (Fig. 1*E*). As astrocytes lack mRNA for BDNF (Ernfors et al., 1990; Conner et al., 1997), these data suggest that *pro*BDNF was taken up by these cells upon secretion from nearby activated neurons. Notably, *pro*BDNF immunoreactivity was typically punctate

within astrocytic processes in contact with nearby neurons, whereas it appeared to be concentrated in larger clusters in the cell body (Fig. 1*E*). This immunoreactivity pattern suggests intracellular trafficking of *pro*BDNF after its transfer from nearby neurons to astrocytes at sites of neuron-glia contacts. We thus decided to follow the time course of *pro*BDNF distribution within astrocytes after TBS (Fig. 1*F*). *Pro*BDNF uptake in individual astrocytes was determined by measuring colocalization of *pro*BDNF immunoreactivity with that of the glial fibrillary acidic protein (GFAP), an astrocytic-specific cytoskeletal protein. In accordance with a transfer of *pro*BDNF from neurons to astrocytes, colocalization of *pro*BDNF to GFAP was first found within the periphery of astrocytic processes 5 min after TBS. At later time points (10-30 min), the overall quantity of *pro*BDNF found in astrocytes had increased, and the intracellular distribution gradually shifted from the processes to the cell body. Finally, *pro*BDNF levels returned to basal levels in both compartments after 3 h. Although astrocytes were largely devoid of *pro*BDNF under basal stimulation, 10-12% of GFAP-labeled individual astrocytes were positive for *pro*BDNF 10 min after TBS (Fig. 2*A* and *B*). This effect was prevented by prior incubation with anisomycin, indicating that accumulation of *pro*BDNF in astrocytes required activity-dependent synthesis in neurons, or with TrkB-Fc, a scavenger for secreted BDNF in both precursor and *mature* forms (Fayard et al., 2005). Strikingly, the astrocytic uptake was selective for *pro*BDNF, as it was markedly reduced upon prior incubation with plasmin (Fig. 2*A* and *B*), an enzyme responsible for the extracellular proteolysis of *pro*BDNF to *mature* protein (Pang et al, 2004).

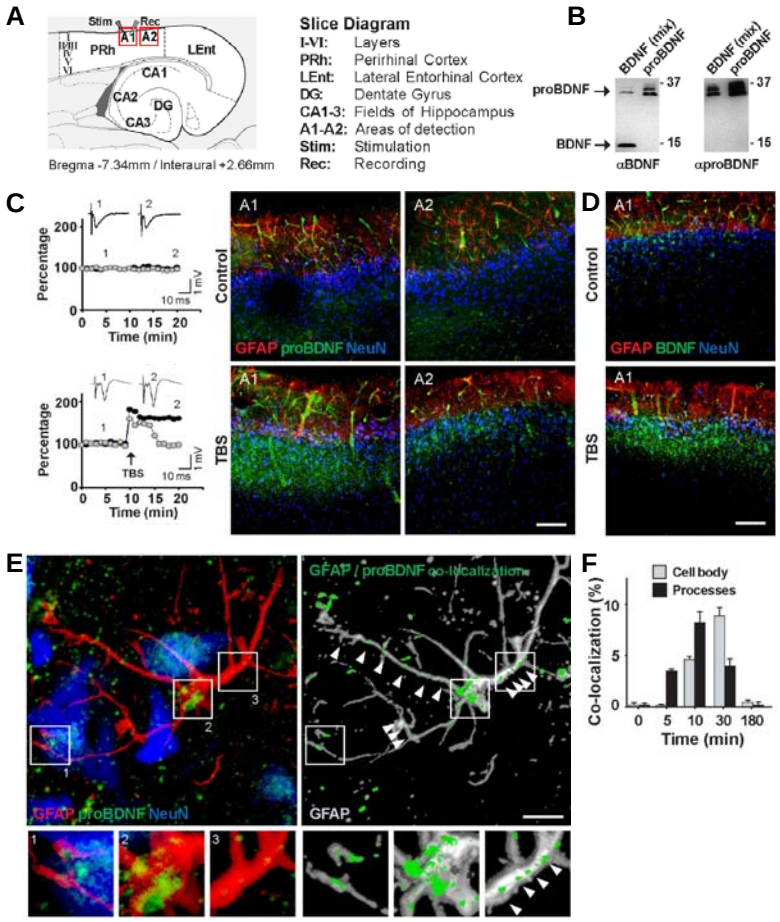

Figure 1. **Transfer of *pro*BDNF from neurons to perineuronal astrocytes.** ***(A)*** Schematic representation of the slice preparation. ***(B)*** Western blot analysis of BDNF (mix) or cleavage-resistant *pro*BDNF (Mowla et al, 2001) using α-BDNF or α-*pro*BDNF specific antibodies. ***(C)*** Field potential amplitudes (black circles) and BDNF levels (gray circles) upon basal (control) or TBS stimulations. After recording, slices were immunostained using α-*pro*BDNF. Immunoreactivity is shown in two adjacent areas corresponding to regions A1 and A2 of ***A***. ***(D)*** Immunostaining made by using α-BDNF. Bar, 100 µm. ***(E)*** High resolution confocal images of region A1 in a slice 20 min after TBS. *pro*BDNF immunoreactivity is shown at the site of astrocytic contacts with a neuron (box and inset 1), astrocytic cell body (box and inset 2), and processes (box and inset 3). Co-localization of *pro*BDNF with GFAP immunoreactivity is shown and superimposed onto the 3D reconstruction of the GFAP signal. Arrowheads indicate *pro*BDNF immunoreactive puncta distributed along the astrocytic processes. NeuN, neuronal nuclei. Bar, 20 µm. ***(F)*** Time course of *pro*BDNF/GFAP co-localization (4 slices and 9 cells).

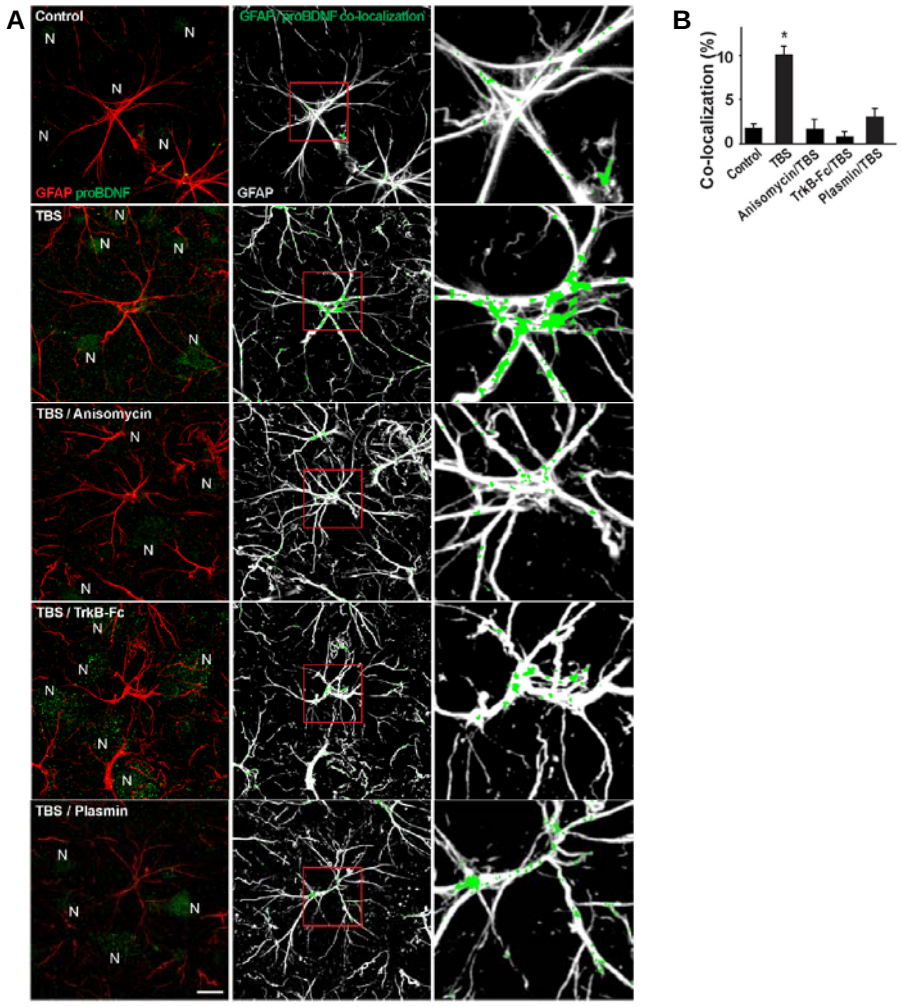

Figure 2. **Transfer of *pro*BDNF to perineuronal astrocytes depends on neuronal protein synthesis and secretion.** ***(A)*** *pro*BDNF/GFAP co-localization in astrocytes of control and TBS slices in presence of anisomycin, TrkB-Fc or plasmin. The immunoreactive signal of co-localized *pro*BDNF was superimposed to the tri-dimensional reconstruction of GFAP positive astrocytes (middle column); high magnifications of cell bodies are shown on the right column. Bar, 20 µm. ***(B)*** Quantification of *pro*BDNF/GFAP co-localization in astrocytes of control (3 slices and 12 cells) or TBS slices in absence (6 slices and 24 cells) or presence of anisomycin (5 slices and 11 cells), TrkB-Fc (4slices and 9 cells), and plasmin (5 slices and 24 cells) 10 min after stimulation. N represents neuronal cell bodies. (*, $P \leq 0.05$).

1.2 p75^{NTR} and clathrin mediate internalization of *pro*BDNF in astrocytes

We next investigated whether *pro*BDNF uptake by astrocytes occurs by receptor-mediated internalization. We observed that *pro*BDNF immunoreactivity within astrocytes colocalized with that of p75^{NTR} 10 min after TBS. Clusters of *pro*BDNF-p75^{NTR} were found at sites in contact with nearby neurons and astrocytic processes, a pattern suggestive of p75^{NTR}-mediated internalization of *pro*BDNF (Fig. 3*A*). Accordingly, in slices of p75^{NTR} knockout mice (p75$^{NTR–/–}$; Naumann et al, 2002) and different from slices of wild-type mice (p75$^{NTR+/+}$), *pro*BDNF did not accumulate in astrocytes (Fig. 3*B* and *C*). However, preventing TrkB internalization with the kinase inhibitor K252a did not affect GFAP/*pro*BDNF colocalization (Fig. 4*B and C*), which is consistent with the notion that astrocytes do not express the full-length form of TrkB (Rose et al., 2003). Because data obtained in slices do not rule out the involvement in BDNF endocytosis of truncated TrkB (TrkB-t) forms (Rubio, 1997) lacking the catalytic domains (Klein et al, 1990), experiments were extended to primary cultures of cortical astrocytes. Surface biotinylation experiments showed that, in addition to p75^{NTR}, cultured astrocytes express TrkB-t but not full-length TrkB (Fig. 3*D*). However, upon exposure of astrocytes to BDNF, a mixture of precursor and mature isoforms (mix; Fig. 1*B*), only the membrane expression of p75^{NTR}, but not TrkB-t, was reduced. As a consequence, the same lysate in which plasma membrane levels of p75^{NTR} were reduced by BDNF (mix) contained a high quantity of BDNF protein. Altogether, these data indicate that *pro*BDNF uptake occurs primarily by p75^{NTR}, which is consistent with the notion that *pro*BDNF binds preferentially to this receptor (Teng et al, 2005). To further investigate the molecular mechanism of *pro*BDNF-p75^{NTR}-mediated internalization, we examined whether endocytic *pro*BDNF colocalized with clathrin (Bronfman et al., 2003). We found that clathrin immunoreactivity colocalized with that of *pro*BDNF after TBS (Fig. 4*A*). This effect was blocked by prior treatment with the clathrin inhibitor monodansylcadaverine (MDC) or the dynamin blocker D15 (Fig. 4*B* and Fig. 4*C*; Wigge and McMahon, 1998). Likewise, we observed colocalization of *pro*BDNF with the early endosomal marker EEA1 (Fig. 4*A*). Overall, these data provide

evidence that astrocytic uptake of endogenous *pro*BDNF occurs via $p75^{NTR}$ and clathrin-mediated internalization in endocytic compartments.

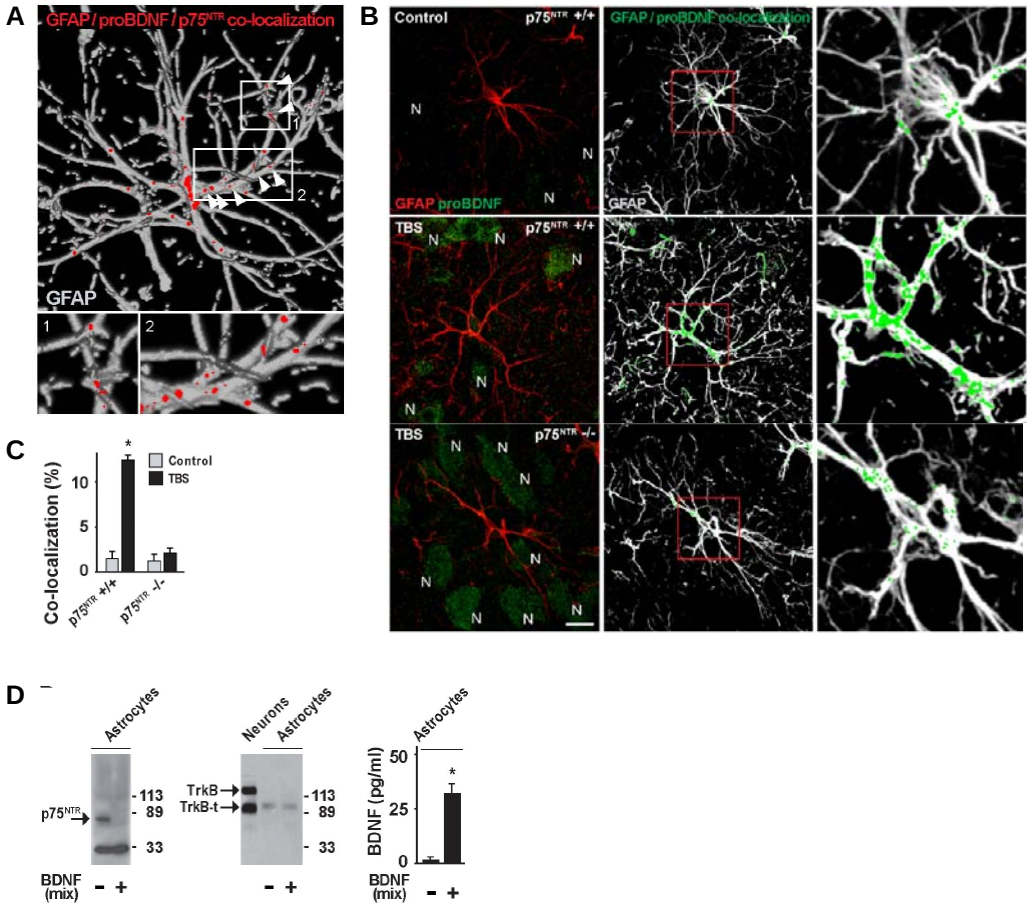

Figure 3. **p75^{NTR}-dependent internalization of *pro*BDNF in astrocytes.** ***(A)*** Colocalization between GFAP, *pro*BDNF and p75^{NTR} immunoreactivity in astrocytes 10 min after slice exposure to TBS. Co-localization signal is shown at the site of astrocytic contact with a neuron (box and inset 1) and astrocytic processes (box and inset 2). Bar, 10 µm. ***(B)*** *pro*BDNF/GFAP co-localization in astrocytes of control and TBS slices of p75^{NTR} +/+ and p75^{NTR} -/- mice. Co-localized signal was superimposed to the tri-dimensional reconstruction of GFAP positive astrocytes (middle column); high magnifications of cell bodies are shown on the right column. N represents neuronal cell bodies. Bar, 20 µm. ***(C)*** *pro*BDNF/GFAP co-localization in astrocytes of control (5 slices and 22 cells) or TBS slices (5 slices and 18 cells) in p75^{NTR} +/+ and p75^{NTR} -/- mice. ***(D)*** Western blot showing surface expression of p75^{NTR}, TrkB, or TrkB-t from control astrocytes or astrocytes exposed to BDNF (mix). TrkB and TrkB-t expression from cultured neurons is shown for comparison. The right panel shows ELISA measurement of BDNF concentration in astrocytes. (*, $P \leq 0.05$).

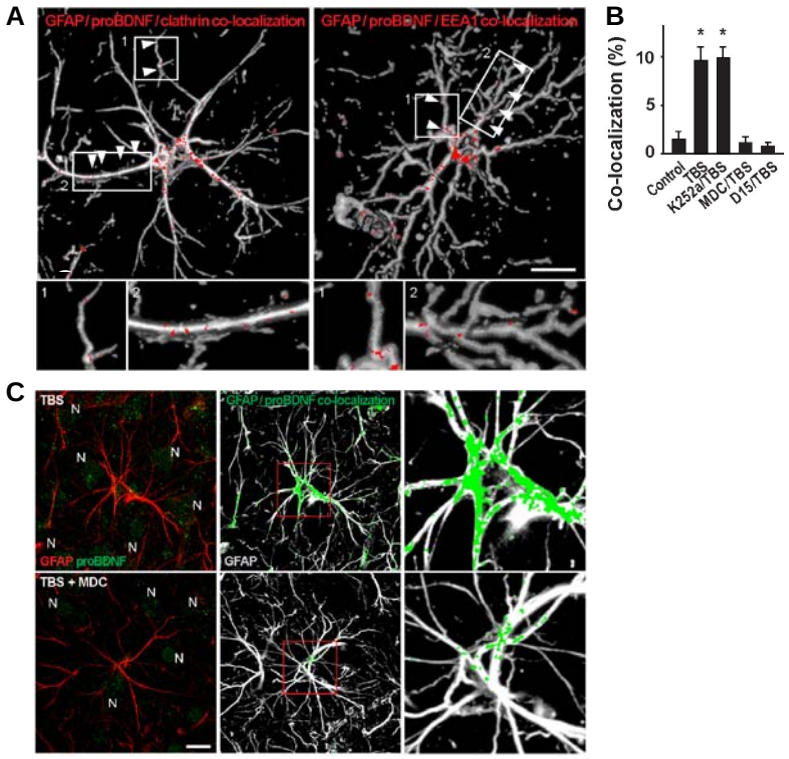

Figure 4. **Astrocitic *pro*BDNF uptake is mediated by clathrin.** ***(A)*** Colocalization between GFAP, *pro*BDNF and clathrin or EEA1 immunoreactivity in astrocytes 10 min after slice exposure to TBS. Co-localization signal is shown at the site of astrocytic contact with a neuron (box and inset 1) and astrocytic processes (box and inset 2). Bar, 10 µm. ***(B)*** *pro*BDNF/GFAP co-localization in astrocytes of control (6 slices and 9 cells) or TBS slices in the absence (4 slices and 12 cells) or presence of K252a (4 slices and 9 cells), MDC (3 slices and 11 cells), or D15 (3 slices and 11 cells). (*, $P \leq 0.05$). ***(C)*** *pro*BDNF/GFAP co-localization in astrocytes of TBS slices in absence or presence of the clathrin inhibitor MDC. Co-localized signal was superimposed to the tri-dimensional reconstruction of GFAP positive astrocytes (middle column); high magnifications of cell bodies are shown on the right column. N represents neuronal cell bodies. Bar, 20 µm.

1.3 Internalization of p75^{NTR}-*pro*BDNF complexes in cultured astrocytes

To obtain further insight into the possible regulation of *pro*BDNF uptake in astrocytes, total internal reflection fluorescence (TIRF) microscopy (Thompson and Steele, 2007) was used to visualize the formation of single endocytic vesicles in real time (Fig. 5*A* and Video 1). Cultured astrocytes were transfected with p75^{NTR} tagged with GFP (p75-GFP) for evanescent light excitation of p75-GFP residing within or in close proximity to the plasma membrane. The binding of *pro*BDNF to p75-GFP was imaged in real time using *pro*BDNF immunocomplexed with 10 nM of quantum dots (QDs; Fig. 5*E*). Once a *pro*BDNF-QD was found in the vicinity of the plasma membrane of a p75-GFP expressing astrocyte, p75-GFP fluorescence became concentrated at the site of the QD within a few seconds, presumably reflecting the formation of endocytic vesicles and internalization of the *pro*BDNF-QDs. Confocal microscopy showed that internalization of *pro*BDNF-QDs was inhibited at a non permissive temperature (ice cold) for endocytosis and was restored by raising the temperature to 37°C for 10-20 min (Fig. 5*B*). QD uptake also depended on the level of p75^{NTR} expression: although astrocytes overexpressing p75-GFP showed high levels of QD internalization, significantly fewer QDs were taken up in astrocytes transfected with plasma membrane-linked GFP (Lck-GFP), which only relies on endogenous p75^{NTR} for internalization (Fig. 5*B* and *D*). Likewise, QD uptake was virtually abolished in astrocytes prepared from p75$^{NTR-/-}$ mice (Fig. 5*C*). Moreover, QD internalization required prior coupling to *pro*BDNF, as it ceased when the α-*pro*BDNF antibody was omitted from the immunocomplexes for control (Fig. 5*B*). Lastly, internalized QDs colocalized with clathrin and EEA1 (Fig. 5*G*), confirming in primary cultures the mechanism of *pro*BDNF endocytosis shown in stimulated slices.

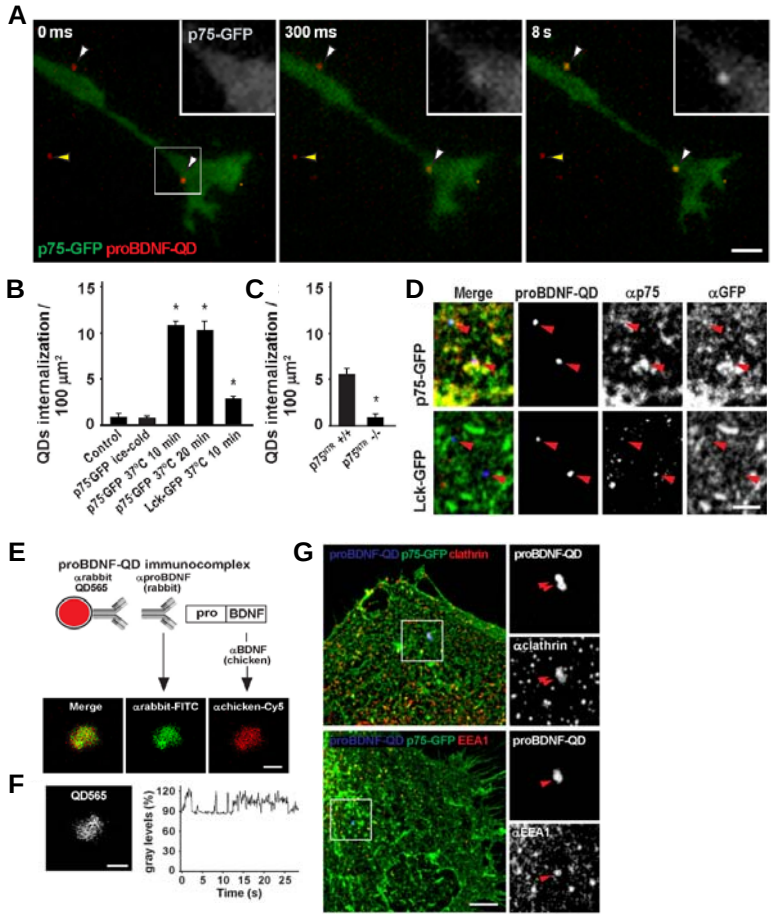

Figure 5. **Internalization of *pro*BDNF-p75^{NTR} complexes in cultured astrocytes.** ***(A)*** Time sequence of *pro*BDNF-QD/p75-GFP internalization in cultured astrocytes by TIRF imaging. White arrowheads indicate *pro*BDNF-QD (red) in close proximity to the membrane of an astrocyte transfected with p75-GFP (green). The yellow arrowhead points to a reference QD. Insets depict p75-GFP fluorescence that concentrates at the site of the QD. Bar, 5 µm. ***(B)*** Quantification of *pro*BDNF-QD internalization in astrocytes transfected with p75-GFP (9 cells) or Lck-GFP (6 cells). ***(C)*** *pro*BDNF-QD internalization in astrocytes from p75^{NTR} +/+ (22 cells) and p75^{NTR} -/- (11 cells) mice. ***(D)*** Confocal pictures showing co-localization (arrowheads) between *pro*BDNF-QDs (blue) and p75^{NTR} (red) in astrocytes transfected with p75-GFP or Lck-GFP (green). Bar, 2 µm. (*, P ≤ 0.05). ***(E)*** Schematic representation of *pro*BDNF-QD immunocomplex. Bar, 0.5 µm. ***(F)*** Intensity profile of *pro*BDNF-QD fluorescence (blinking). Bar, 0.5 µm. ***(G)*** Co-localization between *pro*BDNF-QDs (blue) and clathrin or EEA1 (red) in cultured astrocytes expressing p75-GFP (green). Magnification of selected areas (white boxes) shows QD particles (red arrowheads) co-localized with clathrin or EEA1 immunoreactivity. Bar, 5 µm.

1.4 Regulated secretion of internalized *pro*BDNF by astrocytes

We next addressed the fate of internalized *pro*BDNF. The sorting of endocytic vesicles has been suggested to lead to either vesicle recycling or vesicle entering the degradation pathway (Maxfield and McGraw, 2004; Soldati and Schliwa, 2006). This prompted us to investigate whether internalized *pro*BDNF can eventually be recycled for regulated secretion. To this end, cultures were incubated for 10 min with a mixture of both precursor and mature BDNF tagged with YFP (BDNF-YFP mix; Fig. 6*A*). Internalized BDNF-YFP showed a punctate pattern concentrated at the cell periphery of cultured astrocytes (Fig. 6*B*). Ultrastructural characterization by pre-embedding experiments using immunogold-labeled BDNF-YFP (BDNF-YFP gold; Fig. 6*D*) disclosed gold particles within vesicular structures (mean diameter, 125 ± 22 nm; n = 32; Fig. 6*C*). Whether vesicles containing internalized BDNF-YFP are eventually destined for recycling was next evaluated by exploiting the pH sensitivity of BDNF-YFP. YFP fluorescence quenching inside acidic compartments followed by its unquenching upon BDNF-YFP secretion into the extracellular medium revealed fluorescent flashes by TIRF imaging. After loading astrocytes by brief exposure (1–5 min) to BDNF-YFP (mix), fluorescent vesicles appeared near the plasma membrane (Fig. 6*E* and Video 2). Challenging astrocytes with glutamate triggered flashes lasting several hundred milliseconds. Only when fluorescence increased, spread, and subsequently declined the flash was considered an exocytic event. Quantitative analysis demonstrated that glutamate induced about a 10-fold increase in exocytic events (73 ± 12 mean flashes/astrocyte ± SD; n = 18) with respect to the control bath solution (6 ± 3 mean flashes/astrocyte ± SD; n = 6; Fig. 6*G*). Most of the fusion events took place during the first 10 s of glutamate application. Because recycling is visualized by TIRF rapidly after exogenous BDNF-YFP administration, it is likely that endocytic vesicles containing BDNF-YFP can enter the exocytic process directly. Thus, endocytic vesicles may represent the main storage compartment for endocytosed BDNF-YFP before routing to the secretory pathway. Lastly, neurotrophin recycling was determined by ELISA measurement of BDNF in supernatants collected from cultured astrocytes or astrocytes exposed to BDNF (mix) for 10 min and thoroughly washed (Fig. 6*H*).

Although challenge with glutamate for 5 min did not result in endogenous BDNF secretion from control cells, the same stimulation increased the neurotrophin secretion in BDNF preincubated cells. Neurotrophin release was strongly reduced by overnight intoxication with 40 nM tetanus neurotoxin (TeNT), a protease known to cleave the SNARE protein vesicle-associated membrane protein 2 (Vamp2)/synaptobrevin2 (Montana et al., 2006) and implicated in the regulated release of neurotransmitters from astrocytes (Bezzi et al., 2004). The effect of glutamate was mimicked by 50 μM AMPA or 100 μM t-ACPD, which activate AMPA or metabotropic group I/II glutamate receptors, respectively (Fig. 6*I*). BDNF secretion induced by AMPA or t-ACPD was heavily reduced by the AMPA antagonists CNQX or by the metabotropic group I receptor antagonist AIDA. High frequency (50 Hz) electrical stimulation, which is known to trigger secretion of BDNF in cultured neurons (Balkowiec and Katz, 2000), was not effective (Fig. 6*I*), indicating that BDNF secretion from astrocytes cannot be directly regulated by activity.

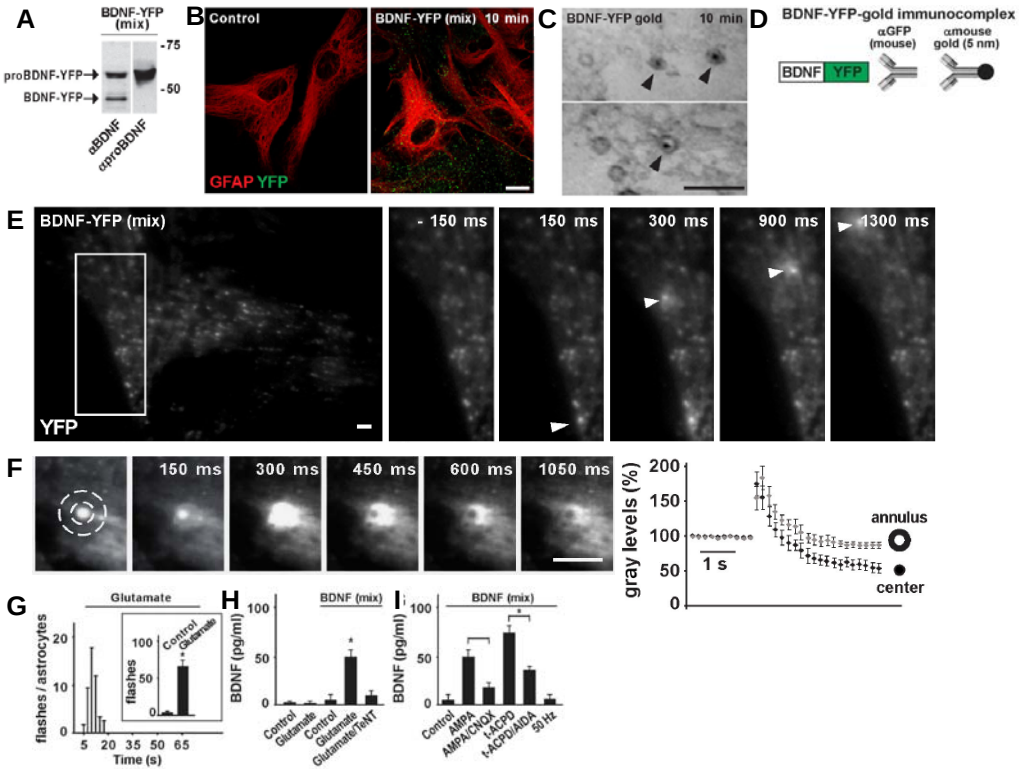

Figure 6. **Astrocytes recycle endocytic *pro*BDNF for regulated secretion.** ***(A)*** Western blot analysis of BDNF-YFP (mix) using α-BDNF or α-*pro*BDNF antibodies. ***(B)*** Immunocytochemistry performed in astrocytes untreated (n = 12) or incubated for 10 min with BDNF-YFP (mix; n = 18) followed by acid strip. Bar, 10 µm. ***(C)*** Electron micrographs of astrocytes exposed to BDNF-YFP gold for 10 min. Arrowheads point to gold particles contained in vesicular organelles. Bar, 500 nm. ***(D)*** Schematic representation of BDNF-YFP gold immunocomplexes used for trateing astrocytes in ***(C)***. ***(E)*** Representative TIRF images of astrocytes incubated with BDNF-YFP for 5 min. The sequence depicts exocytic fusion events (arrowheads) of a selected astrocytic area (white rectangle) after perfusion with glutamate. Bar, 2 µm. ***(F)*** Images sequence showing the fusion process of a single vesicle. Fluorescence intensity (graph on the right) is measured in a circular mask centered over the vesicle and in a concentric annulus on the circle. Bar, 2 µm. ***(G)*** Time distribution of fusion events (flashes) after glutamate application. The inset shows the total number of flashes per astrocyte before (n = 17) and after (n = 13) glutamate application. ***(H)*** ELISA quantification of endogenous BDNF secretion before (n = 18) and after (n = 22) glutamate application. Astrocytes previously exposed to BDNF (mix) for 10 min were stimulated with glutamate in the absence (n = 14) or presence (n = 4) of TeNT. ***(I)*** Secretion of BDNF induced by AMPA or t-ACPD in absence (n = 23) or presence (n = 17) of the respective antagonists CNQX or AIDA and by 50 Hz (n = 6). (*, $P \leq 0.05$).

1.5 SNARE-dependent exocytosis of *pro*BDNF by astrocytes

How is the endocytic *pro*BDNF recycled for exocytosis? One potential mechanism making endocytic vesicles available for secretion involves the molecular machinery deputed to exocytic fusion. Astrocytes are known to express components of the core SNARE complex, including Vamp2 (Montana et al, 2006). Colocalization of *pro*BDNF with Vamp2 was detected within astrocytes in slices 10 min after TBS (Fig. 7*A*) or in cultured astrocytes transfected with p75-GFP and exposed to *pro*BDNF-QDs (Fig. 7*B*). The expression of Vamp2 on BDNF-containing vesicles was confirmed by Western blot analysis of endocytic vesicles purified by magnetic beads coated with α-$p75^{NTR}$ antibodies (Fig. 7*C*). Conversely, endocytic vesicles purified using beads coated with α-Vamp2 antibodies were immunoreactive for $p75^{NTR}$. Interestingly, treatment with BDNF (mix) for 10 min enhanced the recovery of vesicles expressing both Vamp2 and $p75^{NTR}$. Beads coated with antibodies against the neuronal marker microtubule-associated protein 2 (Map2) were used as a control. These data indicate that endocytic vesicles expressing $p75^{NTR}$ may represent the main storage compartment for endocytosed *pro*BDNF before routing to the secretory pathway. This process might take place either by recycling of *pro*BDNF-$p75^{NTR}$ complexes to the surface or by *pro*BDNF recycling upon its dissociation from $p75^{NTR}$. Moreover, given that TeNT prevented BDNF secretion (Fig. 6*H*), all these data indicate that after endocytosis in astrocytes, vesicles containing the neurotrophin may undergo regulated recycling via a SNARE-dependent mechanism.

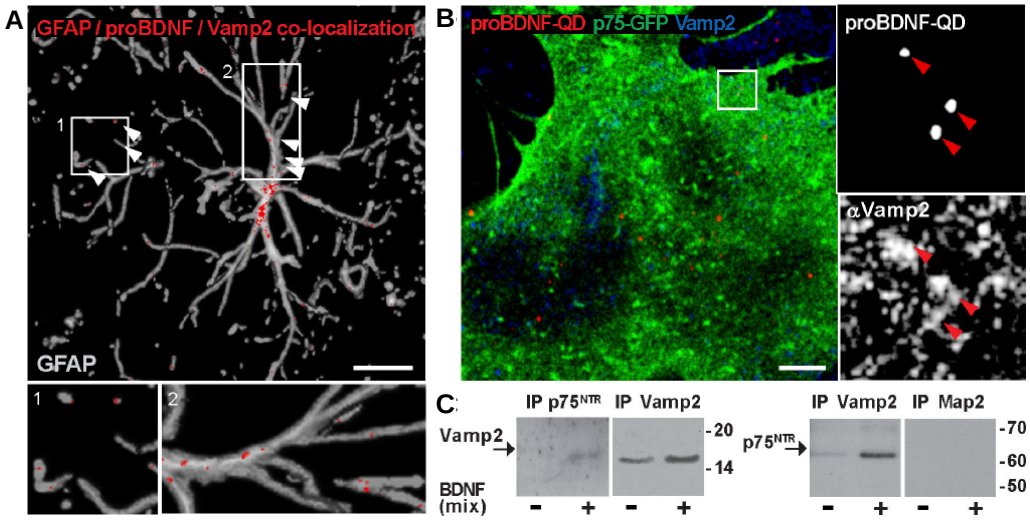

Figure 7. **Vesicles containing *pro*BDNF-p75^{NTR} express the Vamp2 component of the SNARE core complex for vesicle fusion.** ***(A)*** Co-localization between GFAP, *pro*BDNF, and Vamp2 immunoreactivity in astrocytes 10 min after TBS. Co-localization signal (arrowheads) is shown at the site of astrocytic contacts with a neuron (box and inset 1) and astrocytic processes (box and inset 2). Bar, 20 μm. ***(B)*** Immunocytochemistry of cultured astrocytes transfected with p75-GFP showing co-localization between *pro*BDNF-QDs and Vamp2. Right panels depict QD/Vamp2 co-localization (arrowheads) in a selected astrocytic area (boxed area). Bar, 2 μm. ***(C)*** Western blot showing p75^{NTR} and Vamp2 expression in endocytic vesicles immunopurified (IP) by magnetic beads coated with α-p75^{NTR} , α-Vamp2, or α-Map2 from astrocytes untreated or treated with BDNF (mix).

1.6 Hippocampal neurons recycle BDNF for activity-depend secretion and LTP maintenance

So far we have shown that the delivery of high-frequency stimulation in cortical slices induces a conspicuous secretion of *pro*BDNF, which can be detected within few minutes in perineuronal astrocytes. However, the contribution of BDNF to synaptic potentiation is principally due to the availability of its mature form. Previous works have demonstrated that secreted *pro*BDNF can be cleaved extracellularly by plasmin in an activity-dependent manner, thereby allowing the induction and maintenance of LTP (Pang et al, 2004). Here, we test the possibility that biologically active BDNF, which had exert its function during LTP induction, can be locally re-used by the same synapses upon TrkB-mediated uptake and re-secretion for maintenance of the potentiation. We initially demonstrated that BDNF is internalized in large endocytic vesicles in cultured hippocampal neurons via a TrkB-dependent mechanism, and promptly becomes re-available for activity-dependent secretion (BDNF recycling). Most importantly, the recycled BDNF fulfils the function of the newly synthesized BDNF in mediating the conversion of early- into late-phase LTP. We first confirmed in adult (4–6 weeks old) rat hippocampal slices that BDNF is a necessary protein synthesis product for LTP maintenance, as already observed in mice by Pang et al (2004). Field excitatory post-synaptic potentials (EPSPs) evoked by stimulation of Schaffer collaterals were recorded in CA1 area (Fig. 6*A*). TBS induced LTP that persisted for more than 180 min. When the slices were treated for 30 min before stimulation and throughout the recording with the protein synthesis inhibitor anisomycin, the duration of LTP decreased to about 70-100 min. We found that this effect was fully reversed by exogenous BDNF (100 ng/ml) application from 5 min before to 15 min after TBS. The same BDNF treatment was ineffective in the absence of TBS (Fig. 6*G*). To verify whether secretion of endocytosed BDNF could rescue LTP impaired by protein synthesis inhibition, we incubated the slices with both anisomycin (90 min) and BDNF (60 min) before transferring them to the recording chamber in which BDNF was no longer present. Immunohistochemical analysis revealed that this preincubation augmented intracellular BDNF immunoreactivity in neurons in comparison with

untreated slices or slices incubated only with anisomycin (Fig. 6*E*). High-magnification confocal analysis of single optical images (z resolution <1 μm) revealed that immunostaining for BDNF was localized in CA1 pyramidal neuron cell bodies and processes as a punctate intracellular pattern (Fig. 6*F*). Notably, the blocking action of anisomycin on LTP was fully prevented in BDNF-incubated slices (Fig. 6*A* and *B*), suggesting that LTP maintenance could be due to TBS-induced secretion of previously endocytosed BDNF. This interpretation is confirmed by the observation that the effect of BDNF incubation on LTP was abolished (Fig. 6*C* and *D*) by preventing BDNF internalization in slices with K252a or with the PI3K inhibitor LY294002 (Fig. 6*E*), which prevents BDNF and TrkB internalization in cultured neurons as well. A similar effect was obtained by scavenging extracellular BDNF with TrkB-Fc applied from 10 min before to 15 min after TBS (Fig. 6*B*).

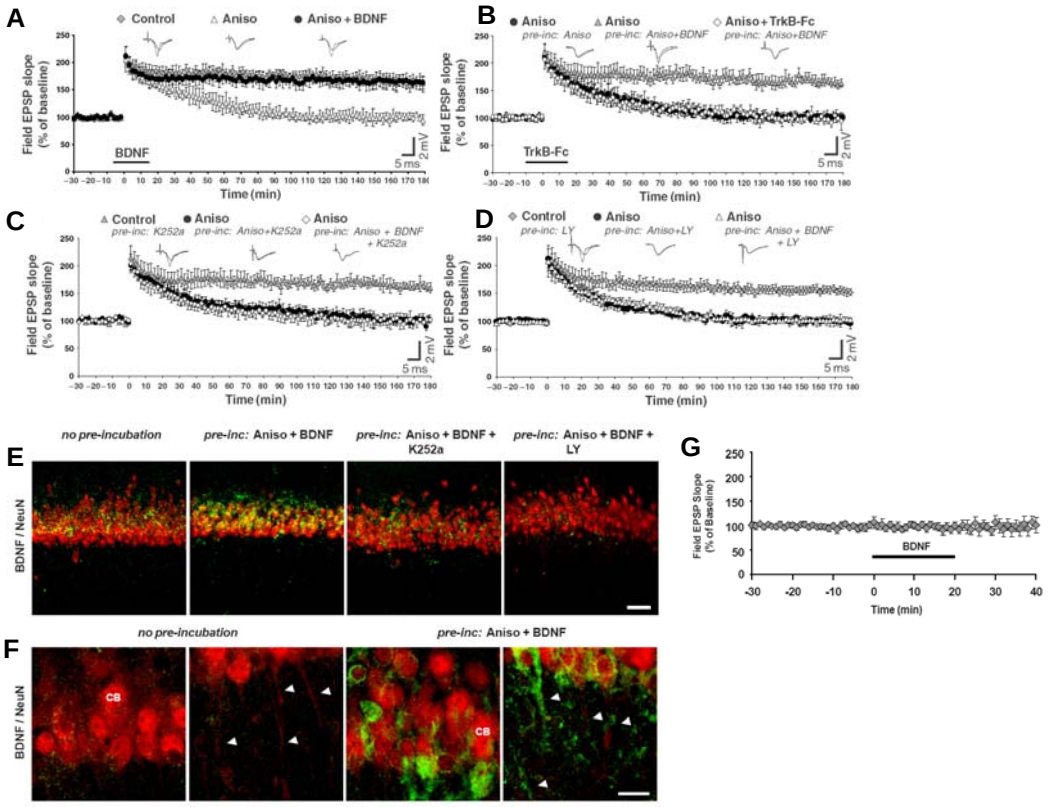

Figure 6. **Endocytosed BDNF rescues LTP impaired by protein synthesis inhibition.** ***(A)*** Field EPSPs evoked in CA1 area by Schaffer collaterals stimulation and plotted as fEPSPs slope percentages of the baseline. On top are shown representative traces recorded before and 180 min after TBS (time zero). LTP was induced in control slices or slices perfused with anisomycin (Aniso) from 30 min before TBS to the end of the recording (5 slices, 5 rats). BDNF was applied as indicated (Aniso+BDNF) (6 slices, 5 rats). ***(B)*** LTP induced in slices incubated either with anisomycin (*pre-inc*: Aniso; 9 slices, 7 rats) or anisomycin and BDNF (*pre-inc*: Aniso+BDNF; 12 slices, 9 rats) in absence or presence (8 slices, 6 rats) of TrkB-Fc (Aniso+TrkB-Fc). ***(C)*** LTP induced in slices incubated either with K252a (*pre-inc*: K252a; 10 slices, 7 rats) or anisomycin plus K252a (*pre-inc*: Aniso+K252a; 9 slices, 6 rats) or anisomycin together with K252a and BDNF (*pre-inc*: Aniso+K252a+BDNF; 11 slices, 8 rats). ***(D)*** Pretreatment with LY294002 (LY) (5 slices, 5 rats) led to the same effects observed in the presence of K252a (panel ***C***). ***(E)*** Representative confocal pictures of CA1 pyramidal cells labelled for BDNF (green) and NeuN (red) in slices incubated with anisomycin and BDNF (*pre-inc*: Aniso+BDNF) with respect to untreated slices (*no pre-incubation)*, and together with K252a (*pre-inc:* Aniso+BDNF+K252a) or LY294002 (*pre-inc:* Aniso+BDNF+LY). Bar, 100 μm. ***(F)*** High magnifications of neuronal cell bodies (CB) and processes (arrows) of control slices or slices incubated with BDNF. Bar, 50 μm. ***(G)*** Lack of effect on basal transmission following 20 min application of 100 ng/ml BDNF.

1.7 Regulated exocytosis of BDNF from Schwann cells

Along with our data describing the trafficking of BDNF in hippocampal and cortical neurons and astrocytes, we investigated whether a similar biological mechanism could also apply to different scenarios, such as the vestibular system, in which the survival of inner ear sensory neurons depends on BDNF (Ernfors et al, 1995; Minichiello et al, 1995). We demonstrated the existence of a functional cross talk between cultured vestibular neurons and Schwann cells lying along their axonal process. In particular, ATP release from vestibular neurons induces calcium transients and BDNF release in Schwann cells expressing $p75^{NTR}$, which in turn plays a trophic role on neurons. In this respect, we have showed the existence of a regulated vesicular release in Schwann cells in response to ATP by real-time imaging. To assess the capacity of these glial cells to undergo regulated secretion in response to ATP, we stained Schwann cells cultures with acridine orange (AO), which has been used to tag vesicles in cultured astrocytes (Bezzi et al., 2004). Following accumulation into vesicular acidic compartments, this dye changes its spectral properties and shifts its emission from green to red light. Total internal reflection fluorescence microscopy (TIRF) has shown that a subpopulation of AO-loaded vesicles undergo rapid membrane fusion following astrocyte stimulation (Bezzi et al., 2004). We used the same approach to investigate the possible existence of vesicle fusion in Schwann cells. Figures 9*A* and *B* show that stimulation with 1 mM ATP induces the fusion of AO positive vesicles with the plasma membrane, resulting in the production of light flashes (arrowheads in Fig. 9*B*). These flashes were followed by lateral spread of fluorescence and, finally, by the disappearance of the labelled organelle (Fig. 9*C*). The number of light flashes observed during a 3 min application of ATP were increased roughly 10-fold with respect to buffer application only. To assess the dependence of these fusion processes on SNARE proteins, Schwann cells were intoxicated overnight with 40 nM Tetanus Toxin, which proteolyzes synaptobrevin/VAMP2 and cellubrevin and blocks exocytosis in both neurons and astrocytes (Parpura and Chapman, *2005*; Schiavo et al., 2000). TeNT intoxication prevented the occurrence of AO-positive flashes induced by ATP

stimulation (not shown), thus indicating that, similarly to astrocytes, vestibular Schwann cells possess organelles, which undergo SNARE-dependent regulated fusion with the plasma membrane. Subsequent measurments of BDNF levels in the supernatant of Schwann cells after exposure to ATP and in absence or presence of TeNT intoxication, demonstrated that the vescicular fusions observed in TIRM represent the mechanism through which BDNF is released.

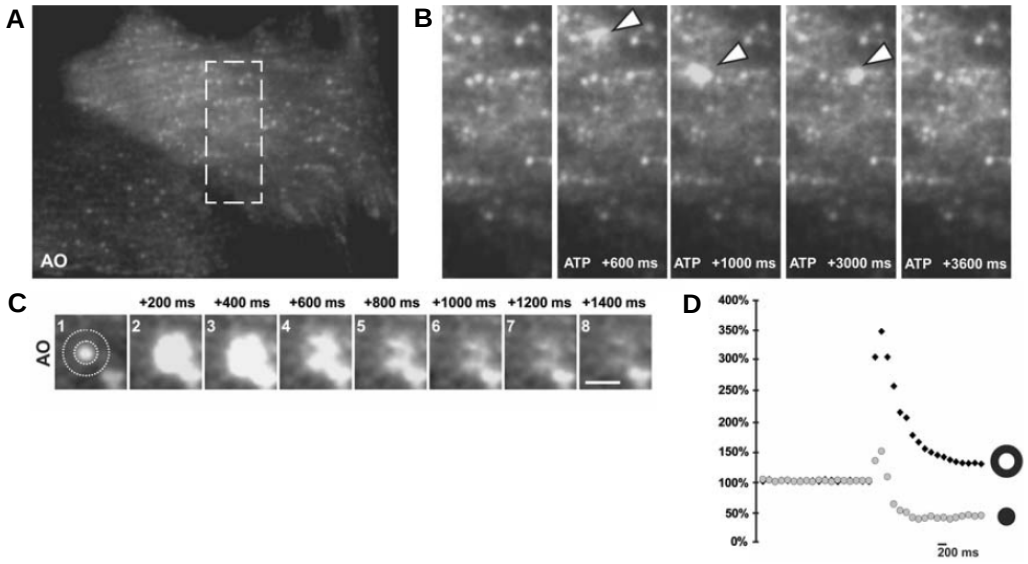

Figure 8. **ATP-induced exocytotic release from Schwann cells.** ***(A)*** Fusion of vesicles analyzed by TIRF imaging in Schwann cells incubated with AO for 3 min. ***(B)*** Sequence of images showing flashes of AO fluorescence (arrows) within a selected area of a single cell. Times indicate the milliseconds elapsed after ATP application. ***(C)*** Sequential images illustrating the fusion event to the plasma membrane of a single vesicle. Times represent milliseconds from appearance, increase in brightness (200 ms), diffusion (400 ms) and decrease (800 ms) of the fluorescent signals. Bar, 2 μm. ***(D)*** Fluorescence AO intensity (graph on the right) is measured in a circular mask of 60 pixels centered over the vesicles and in a concentric annulus of 120 pixel on the circle. Bar, 2 μm.

1.8 Discussion

1.8.1 Contribution to BDNF availability via neuronal synaptic recycling

A major finding of the present study is that endocytosed BDNF in hippocampal neurons promptly undergoes activity-dependent secretion. Optical and biochemical techniques were used to investigate this process in real time. Time-lapse confocal imaging showed regulated secretion of endocytosed BDNF-YFP in the soma and processes of cultured neurons. Single vesicle dynamics, studied by TIRF imaging, revealed the rapid (milliseconds) fusion of BDNF-YFP-containing vesicles to the plasma membrane already 1 min after exogenous BDNF-YFP administration. Thus, the whole recycling process can occur on a rapid timescale. Finally, ELISA quantification of BDNF in the perfusate of neurons previously incubated with exogenous BDNF disclosed increased BDNF levels upon KCl application or high-frequency electrical stimulation.

The recycling process described here is distinctly different from the long-lasting transfer of endocytosed NTs to distal synapses previously described in the visual system (von Bartheld et al, 1996; Butowt and von Bartheld, 2001; Wang et al, 2002; Butowt and von Bartheld, 2005). Distant transfer of endocytosed NTs requires many hours of NTs transport following internalization, and passage through the same sorting pathway (Golgi system) of the newly synthesized NTs before secretion (reviewed by Lessmann et al, 2003; von Bartheld, 2003). Instead, here we document a process in which BDNF internalized in large TrkB-containing vesicles avoids ER and Golgi and never co-localizes with newly synthesized BDNF before secretion. Endocytic vesicles may thus represent the main storage compartment for endocytosed BDNF, before routing to the secretory pathway. Since recycling can occur rapidly after exogenous BDNF administration, it is likely that endocytic vesicles containing BDNF can enter the exocytic process directly, in contrast with the general assumption that they are not designated for regulated exocytosis. This might take place either by recycling of BDNF–TrkB complexes to the surface, or by BDNF recycling upon its dissociation from TrkB. The rapid recycling of endocytic vesicles also implies that BDNF is re-secreted locally, near the site of endocytosis.

Given that NTs cannot diffuse far from the site of secretion (Blochl and Thoenen, 1995; Wang et al, 1998), recycling may provide a mechanism that contributes to the tight control of BDNF availability in close proximity to TrkB localization. TrkB receptors are known to be expressed in both dendrites and axons (McAllister et al, 1999; Poo, 2001); therefore, BDNF is expected to be recycled by both synaptic partners. This would imply that the amount of recycled BDNF can be controlled by the number of TrkB transferred to the cell surface. Membrane insertion (Du et al, 2000) and internalization (Du et al, 2003) of these receptors at active synapses change dynamically depending on neuronal activity. This is of particular importance as both NT availability and expression of Trk receptors must be tightly regulated and synchronized to transduce NT signaling in synaptic plasticity (McAllister et al, 1999; Poo, 2001).

It is generally accepted that high-frequency neuronal activity stimulates the secretion of BDNF (Balkowiec and Katz, 2000; Hartmann et al, 2001; Aicardi et al, 2004), strengthening and maintaining active synapses (Poo, 2001; McAllister, 2002). In this context, recycling may help to maintain the size of the activity-dependent releasable pool of BDNF. Although obviously dependent on newly synthesized BDNF secretion for an initial supply, activity-dependent recycling may endow neurons with the capacity to re-use BDNF on a rapid timescale depending on demand. This might be particularly important for LTP maintenance, which requires threshold BDNF levels (Korte et al, 1995, 1996; Patterson et al, 1996) secreted during a limited time window after TBS (Aicardi et al, 2004). More direct evidence supporting the role of recycling in LTP maintenance comes from the experiments carried out in hippocampal slices. After pre-incubation with exogenous BDNF, TBS induced the secretion of endocytosed BDNF that rescued LTP impaired by protein synthesis inhibition. Endocytosed BDNF was secreted in tight temporal conjunction with the LTP-inducing electrical stimulation: TrkB-Fc applied from 5 min before up to 15 min after TBS to BDNF-treated slices abolished the rescue of LTP maintenance. This finding is in accordance with previous investigations showing that this time window is critical for BDNF action on LTP (Chen et al, 1999; Aicardi et al, 2004; Pang et al, 2004; for review see Pang and Lu, 2004). Thus, recycling can

replace newly synthesized BDNF secretion in maintaining LTP when adequately supplied.

Another interesting aspect concerns the possible functional difference between endocytosed and newly synthesized BDNF, due to the fact that a substantial portion of the latter is secreted as *pro*-form (Mowla et al, 1999, 2001; Egan et al, 2003; Chen et al, 2004). In contrast to mature processed NTs, the *pro*-form shows preferential binding affinity for the pan-receptor $p75^{NTR}$ with respect to Trk receptors (Lee et al, 2001). There is evidence that secreted *pro*BDNF participates in synaptic modifications only upon its conversion into the *mature* protein by extracellular proteolysis, a process dependent on the concomitant release of tissue plasminogen activator (Pang et al, 2004). The finding that endocytosis of BDNF occurs in hippocampal neurons selectively via full-length TrkB indicates that BDNF is predominantly internalized in its mature form. Thus, BDNF recycling may represent a mechanism for selectively supplying BDNF without further processing to induce synaptic modifications.

1.8.2 Significance of BDNF recycling in cortical astrocytes

A second major finding of the present study is that cortical astrocytes exert an important function in the clearance of *pro*BDNF secreted upon neuronal activity and subsequent recycling of the endocytic neurotrophin, thus regulating both its spatial and temporal availability. Despite the lack of endogenous neurotrophin expression in these cells, recycling discovers astrocytes as a cellular source regulating neurotrophin availability in response to external stimuli. Optical imaging was used to investigate this process in real-time. Time-lapse TIRF analysis and confocal microscopy allowed the direct visualization of *pro*BDNF-QD/p75-GFP complex formation and subsequent internalization in individual endocytic vesicles. Tracking of single vesicles revealed juxtamembrane trafficking of BDNF-YFP encompassing exocytic fusion events. Indeed, the vesicles implicated in this process show structural and molecular properties (both endocytic and exocytic) which are consistent with their fusion-proficiency. Finally, ELISA quantification of BDNF in

the perfusate of astrocytes previously incubated with exogenous BDNF disclosed increased BDNF levels upon glutamate application but not high-frequency electrical stimulation.

The recycling of BDNF occurring in astrocytes is different from that described in neurons. The latter requires internalization of *mature* BDNF via TrkB full-length receptors. In contrast, the finding that endocytosis occurs in astrocytes selectively via $p75^{NTR}$ indicates that these cells predominantly internalize *pro*BDNF (Lee et al, 2001). This diversity implies functional differences related to the availability of *mature* and/or precursor isoforms which may occur during synaptic plasticity. Patterned neuronal stimulation is known to promote secretion of *pro*BDNF (Yang et al, 2008; Nagappan et al, 2009; Mowla et al, 2001), which is required to maintain LTP after its conversion into the *mature* protein by extracellular proteolysis (Pang et al, 2004). Alternatively, activation of $p75^{NTR}$ by *pro*BDNF leads to long-term depression (LTD) (Woo et al, 2005; Rösh et al, 2005). Thus, *pro*BDNF internalization in perisynaptic astrocytes can represent a mechanism for selectively regulating neurotrophin signaling, possibly influencing synaptic modifications. In this context, *pro*BDNF internalization may serve to either scavenge the excess of neurotrophin secreted at synaptic contacts or to supply it back to neurons. Since astrocytes cover specific territories that may account for thousands of synapses (Volterra and Meldolesi, 2005), fractions of these territories can control autonomously, and possibly differently, the fate of the internalized neurotrophin. These microdomains include the dynamic structure filopodia and lamellipodia which we found to be the target of endosomes containing the internalized *pro*BDNF-QD complexes. Moreover, the observation that a subset of these endosomes is constrained at the site of internalization and that undergoes rapid recycling implies a local regulation of neurotrophin availability.

These dynamic features suggest for a tide regulation of neurotrophin-mediated cross-talk between neuron and astrocytes. Our data also indicate that neuronal activity plays a pivotal role in regulating neuron-glia neurotrophin trafficking: first, activated neurons secrete *pro*BDNF which is then captured by contacting astrocytes; second, astrocytes are rapidly responsive to neurotransmitters

in releasing neuroligands (Ref), including the neurotrophin. Since *mature* BDNF is known to facilitate neurotransmitter release from pre-synaptic neurons (Poo, 2001), the ability of astrocytes to make the neurotrophin re-available at active synapses may influence back neuronal activity, suggesting that active synapses will specifically benefit from BDNF recycling. In this constest, astrocytes represent a strategic synaptic compartment where *pro*BDNF proteolisis can occur, since it has been shown that astrocititc endosomes contain the proteases capable to cleave *pro*BDNF into *mature* BDNF (Oh-Hashi et al, 2009). Although we cannot completely work out whether internalized *pro*BDNF is efficiently processed within the astrocitic endosomes before being re-secreted, our data suggest the possibility that astrocytes could cover the function of cleaning up the excess of *pro*BDNF secreted form neurons and then recycle it as mature BDNF in order to modulate the synaptic changes associated to LTP.

In line with this scenario, we demonstrated that secretion of endocytosed BDNF in astrocytes is triggered by glutamate through mechanisms similar to those that we have shown for endocytosed BDNF in hippocampal neurons. The common mechanism underlying the re-secretion from these two sources could therefore be important from a functional point of view: it can ensure that BDNF is recruited by the same patterns of neuronal activity, and thus both cellular supplies of BDNF may synergistically regulate synaptic modifications.

2. Deletion of TrkB in adult progenitors alters newborn neuron integration into hippocampal circuits and increases anxiety-like behavior

2.1 Deletion of TrkB specifically in adult-born neurons

To examine the role of TrkB signaling specifically in adult neurogenesis we took advantage of a recently generated mouse line expressing the inducible form of Cre (CreERT2) in the locus of the astrocyte-specific glutamate transporter (GLAST) (Mori et al, 2006) to induce efficient Cre-recombination by tamoxifen in the radial glia-like stem cells of the dentate gyrus. This mouse line was crossed with homozygous $TrkB^{lox/lox}$ mice (Minichiello et al, 1999) in which the second exon of the TrkB tyrosine kinase region had been flanked by two loxP sites (for simplicity $TrkB^{lox/lox}$-Cre). To visualize the recombined cells we additionally crossed $TrkB^{lox/lox}$-Cre mice with transgenic mice expressing green fluorescent protein (GFP) ($TrkB^{lox/lox}$-Cre Z/EG) or β-galactosidase (βgal) ($TrkB^{lox/lox}$-Cre R26R) reporters (Table 1). Tamoxifen treatment in the resulting mice causes the CreERT2 fusion protein to translocate into the nucleus of GLAST-expressing cells, where it recombines paired loxP sites and removes the catalytically active TrkB (Minichiello et al, 1999) without interfering with truncated TrkB (Klein et al, 1993) (Fig. 1*D*). As expected from previous studies (Mori et al, 2006), mice induced by tamoxifen for 5 days and killed 28 days post-tamoxifen application (28 dptm) showed reporter-positive astrocytes throughout the brain parenchyma and radial glia-like stem cells and their neuronal progeny in the dentate gyrus of the hippocampus (Fig. 1*A*-*C*). However, as mature astrocytes express only truncated TrkB, but not the full-length receptor (Fig. 1*D*), the effect of full-length TrkB deletion was restricted to progenitors and differentiating neurons.

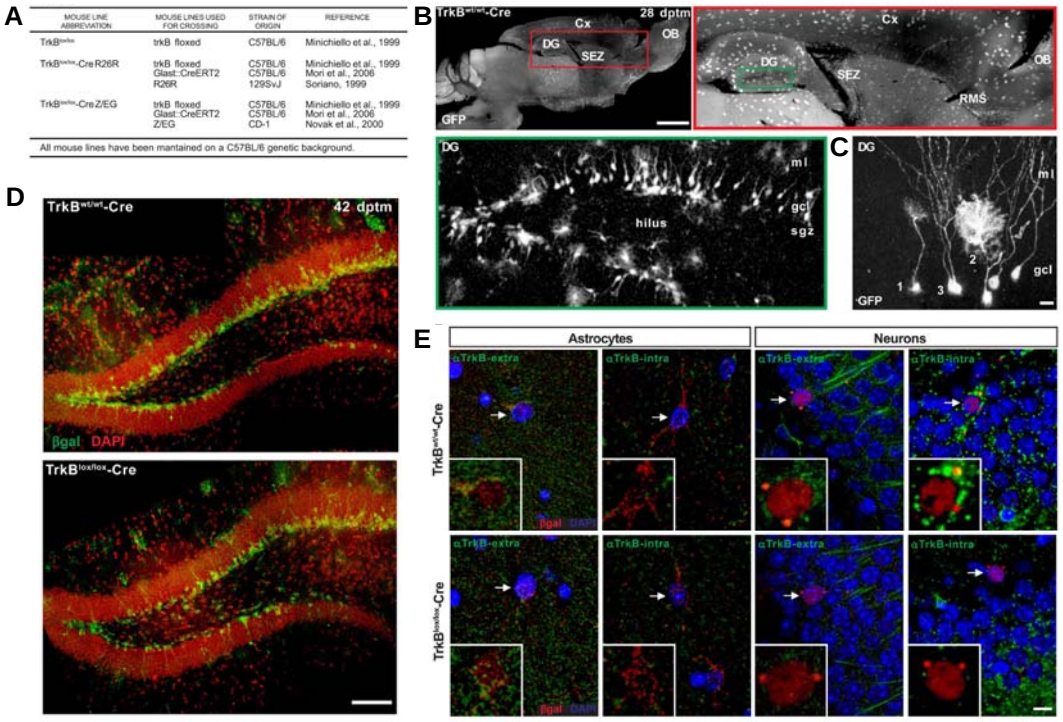

Figure 1. **Characterization of Cre-mediated recombination in the dentate gyrus of TrkB-Cre mice. (*A*)** A table format gives detailed information on the different strains used in each line cross. ***(B)*** TrkB$^{wt/wt}$-Cre Z/EG mice induced by tamoxifen for 5 days and killed 28 days post tamoxifen application (28 dptm) showed reporter positive astrocytes throughout the brain parenchyma as well as radial glia-like stem cells and their neuronal progeny in the dentate gyrus (DG) of the hippocampus. Representative images of a brain section show GFP expression in the dentate gyrus of the hippocampus and the sub-ependymal zone (SEZ) of the lateral ventricle (red rectangle). High magnification of the dentate gyrus (green rectangle) shows a heterogeneous population of marker-positive cells mainly located at the hilar side of the granule cell layer (gcl). Cortex (Cx), olfactory bulb (OB), rostral migratory stream (RMS), molecular layer (ml), subgranule cell layer (sgz). Bar, 2 mm. **(*C*)** Cells expressing the recombination marker in the dentate gyrus of TrkB$^{wt/wt}$-Cre Z/EG mice 28 dptm. GFP+ cells show the morphology of radial glial-like stem cells (1), protoplasmic astrocytes (2), and newborn neurons (3). Bar, 10 μm. **(*D*)** Overall distribution of βgal immunoreactivity in the granule cell layer of the dentate gyrus of the hippocampus in TrkB$^{wt/wt}$-Cre and TrkB$^{lox/lox}$-Cre mouse brain 42 dptm. Bar, 50 μm. **(*E*)** Representative confocal images showing the expression of TrkB receptor in astrocytes and granule cell neurons of TrkB$^{wt/wt}$-Cre and TrkB$^{lox/lox}$-Cre after tamoxifen-mediated recombination. TrkB receptor was stained by using specific antibodies raised against either the catalytic domain of TrkB (αTrkB-intra), which specifically recognizes the full-length receptor, or its extracellular domain (αTrkB-extra), which recognizes both full-length and truncated forms. Bar, 10 μm.

To examine the process of neurogenesis in the dentate gyrus of the hippocampus, the temporal pattern of Cre activity was first investigated in control mice. Mice were induced by tamoxifen for 5 days and analyzed at 1, 28, and 42 dptm (Fig. 2*A*). At each time point we quantified reporter-positive cells identified by cell type-specific antigens (Fig. 2*B*). At 1 dptm the majority of reporter-positive cells expressed the astroglial marker glial fibrillary acidic protein (GFAP), consistent with the recombination occurring specifically in cells with a glial identity. On the contrary, small amount of neuroblasts or immature neurons expressing doublecortin (Dcx) was detectable at this time. Only at later stages did the number of Dcx+ cells increase and reach a plateau at 28 dptm (Fig. 2*A*). At approximately this time, reporter-positive cells started to express the mature neuronal marker NeuN, which transiently overlapped with Dcx. At 42 dptm, most of the NeuN+ cells no longer coexpressed Dcx and by now contributed half of the reporter-positive cell population. Overall, these findings show that neurogenesis follows a typical pattern of progression (Lledo et al, 2006), and manipulations such as Cre activity by tamoxifen treatment in these mice did not alter the temporal maturation stages of newborn neurons.

2.2 TrkB deletion deos not alter precursor cells proliferation

Whether the proliferative steps of neurogenesis can be influenced by TrkB signaling was initially assessed the total number of active proliferating cells, labelled for the cell cycling-associated protein ki67 (ki67+ cells), in $TrkB^{lox/lox}$-Cre and control mice after tamoxifen-mediated recombination occurred (Fig. 3*A)*. The number of ki67+ cells resulted comparable in both experimental groups (Fig. 3*B)*; moreover, we could confirm that the majority of cycling cells was also expressing the reporter marker βgal (βgal+ of ki67+), indicating that these cells properly underwent recombination and that the resulting deletion of TrkB did not impair they survival (Fig. 3*A* and *B*). To evaluate if the proliferative capacities of ki67+ cells was influenced by TrkB deletion, we checked the number of newborn neurons directly generated by ki67+ cells. As these cells reflect the population of fast proliferating cells in the adult dentate gyrus, we labelled them by injecting BrdU for 3 days (Fig.

3*A*) and we checked the number of cells that retained BrdU during this time window as indication of newly generated neurons. Again, similar numbers of labelled cells (BrdU+) were observed in TrkB-deficient and control mice (Fig. 3*B*), suggesting that TrkB is not directly involved in the genesis of new neurons.

2.3 Reduced long-term survival of TrkB-deficient new neurons

To assess whether TrkB signaling influenced the lineage progression of the newly generated cells described above, we examined in detail tamoxifen-induced $TrkB^{lox/lox}$-Cre mice (Fig. 2*A*). At all time points investigated, the fraction of reporter-positive cells expressing GFAP or Dcx was not significantly different from that in control littermates, confirming that the composition of progenitors and new neurons that exit the cell cycle was not altered by deletion of TrkB (Fig. 3*B*). However, at 42 dptm the density of reporter-positive cells expressing the mature neuronal marker NeuN was distinctly reduced in $TrkB^{lox/lox}$-Cre mice (Fig. 2*C*). To further define the precise cell-maturation phase at which TrkB influences the survival of new neurons, we quantified newborn neurons at an earlier developmental stage when they still co-express both Dcx and NeuN. Notably, the density of reporter-positive cells double positive for these markers (Dcx+/NeuN+) decreased significantly 42 dptm (Fig. 2*D*). Moreover, we investigated the TrkB-dependent survival by directly estimating apoptotic cells at the stage we observed reduced cell density. By checking active Caspase-3 positive cells, we demonstrated an increase in the total number of apoptotic cells, with a five fold increase in the number of dying reporter-positive cells co-expressing NeuN (Casp3+/ βgal+/NeuN+) (Fig. 3*C*). Thus, the survival effect mediated by TrkB occurs at the immature-to-mature neuronal transition, corresponding to a critical time after 4 weeks in a neuron's life.

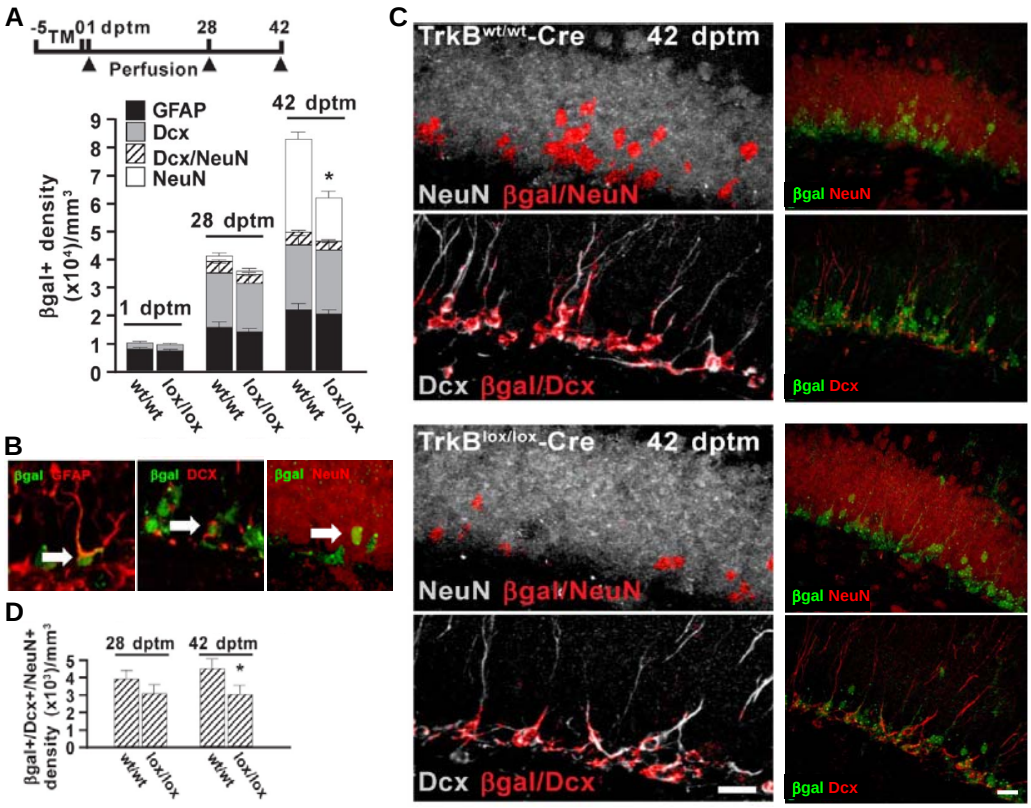

Figure 2. **Deletion of TrkB affects the survival of newborn neurons. (*A*)** Schematic diagram showing the experimental paradigm used for tamoxifen-induced Cre recombination in TrkB$^{lox/lox}$-Cre R26R mice and control littermates. Histograms depict the density distribution of reporter-positive cells (βgal+) expressing GFAP, Dcx, or NeuN in TrkB$^{wt/wt}$-Cre (wt/wt) and TrkB$^{lox/lox}$-Cre (lox/lox) mice. Ten slices per hemisphere and two mice for each time point were analyzed (*****, $p<0.05$). **(*B*)** Representative confocal images of cells co-expressing βgal (green) and GFAP, Dcx or NeuN (red). Bar, 10 μm. **(*C*)** Representative confocal images depict the reporter marker βgal colocalized with either the neuronal marker NeuN (βgal/NeuN) or Dcx (βgal /Dcx). Colocalization signals (red) were superimposed on NeuN or Dcx immunoreactivity (gray). Labeling of single markers from which colocalization was obtained is shown on the right panels Bar, 20 μm. **(*D*)** Density of reporter-positive cells co-expressing Dcx and NeuN (βgal^{+}/ Dcx^{+}/NeuN^{+}) in TrkB$^{wt/wt}$-Cre and TrkB$^{lox/lox}$-Cre as in ***A***. Ten slices per hemisphere and two mice for each time point were analyzed (*****, $p<0.05$).

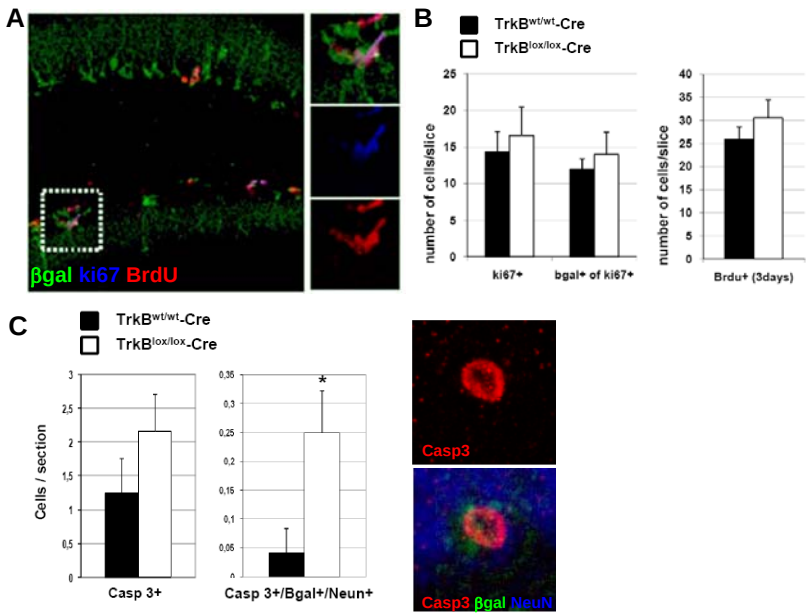

Figure 3. **Survival of newborn neurons, but not proliferation, results affected by deletion of TrkB. (*A*)** Representative confocal picture showing the distribution of recombined proliferating cells stained for the marker ki67 as well as cells which incorporated BrdU after a treatment lasting for 3 days Bar, 50 µm. 3x digital zoom of a selected area (dotted square) is shown on the right panels showing BrdU labeling of proliferating cells. **(*B*)** Histograms showing the quantifications of ki67 positive cells (ki67^{+}) in TrkB$^{lox/lox}$-Cre and control littermates after TM-induced recombination occurred. The majority of proliferating cells also co-express the reporter marker βgal (βgal^{+} of ki67^{+}). The histogram on the right reports on the number of cells which incorporated BrdU (BrdU^{+}) in 3 days of treatment. For both quantifications, 5 slices per hemisphere and 3 mice per group were analyzed (*****, $p<0.05$). **(*C*)** Quantification of apoptotic cells positive for active Caspase-3 (Casp3^{+}) in the granule cell layer of TrkB-deficient and control mice 42 dptm. Apoptotic cells were also identified for the expression of βgal and NeuN (Casp3^{+}/βgal^{+}/NeuN^{+}) as shown on the right panels. Bar, 10 µm.

2.4 Reduced dendritic arbor and spine complexity of TrkB-deficient new neurons

We next investigated whether the integration of adult-born neurons into the existing circuitry would be impaired in the absence of TrkB. As the ability of newborn neurons to integrate involves a progression through distinct morphological stages of maturation (Toni et al, 2007; Zhao et al, 2006) we focused on axon growth, dendritic arborization, spine shape and number, and synapse formation at 28 dptm, the time at which neuronal cell death was not yet apparent. As neurogenesis proceeds continuously, 28 dptm reporter-positive cells consist of a heterogeneous population including precursors and adult-born neurons of mixed age. To establish the exact age of reporter-positive neurons we performed retroviral-birthdating analysis on tamoxifen-induced $TrkB^{lox/lox}$-Cre R26R mice. Mice were injected with retrovirus transducing GFP through stereotaxic delivery into the dentate gyrus of the hippocampus on the fifth day of tamoxifen treatment (Fig. 4*A*), the time immediately preceding the beginning of neurogenesis after Cre recombination.

2.4.1 Axonal growth

At day 28 postinjection (28 dpi) we observed axon fibers labeled by GFP at the inner margin of the CA3 area in the hippocampus (Fig. 4*A*). Axonal length was scored by tracing axon fibers from the dentate to the end of the axons (Zhao et al, 2006). We found that traced lengths were similar in knockout (1002 ± 34 μm; n=11) and control (987 ± 29 μm; n=11) mice, indicating that the elongation and direction of axons projecting to CA3 were independent of TrkB in these neurons.

2.4.2 Dendritic growth

In the same sections we analyzed dendritic growth on transduced neurons extending through the molecular layer of the dentate gyrus. Injection of the virus resulted in a sparse labeling of cells, enabling us to follow detailed changes in dendrite morphology of individual neurons. When confocal analysis followed by three-dimensional reconstruction and morphometric evaluation of the dendritic arbor was carried out in labeled neurons, it was evident that the total number of branches

and dendritic length were significantly reduced in TrkB-deficient vs. control neurons (Fig. 4*B*). Moreover, Sholl analysis (Sholl, 1953) revealed that the dendritic complexity of TrkB-deficient neurons was reduced at sites further than 90 μm from the soma compared with control neurons (Fig. 4*C*). As expected from a previous study (Mori et al, 2006), we observed that recombination occurred in most (~90%) of the newly generated neurons in these mice, but few cells were reporter negative. This permitted us to compare the dendritic morphology of newborn neurons transduced by GFP virus that were recombined (βgal+) with those in which the recombination did not take place (βgal-) in the same section. Strikingly, while βgal- cells expressed features of control neurons the βgal+ displayed thin dendrites that were poorly arborized (Fig. 4 *B-D*). To further evaluate whether the regulation of dendritic growth by TrkB is a ligand-dependent process, we examined dendritogenesis of newborn neurons transduced by GFP virus in heterozygous BDNF knockout mice (BDNF+/-; Korte et al., 1995). Dendritic growth in these mice was previously shown to be impaired in granule neurons of the dentate gyrus, by virtue of reduced BDNF levels (Chen et al., 2006). Indeed, dendritic growth was impaired specifically in newborn neurons (Fig. 4*E*). Interestingly, re-expression of BDNF in new neurons by retroviral injection did not rescue the morphological deficit observed in these mice (Fig. 4*E*), suggesting that BDNF needed for the dendritic growth of adult-born neurons is not selfprovided, but rather, supplied by the surrounding cellular environment. We next examined the specific requirement of TrkB tyrosine kinase signaling on dendritic growth of single adult-born neurons. By injecting a retrovirus transducing both Cre recombinase and the reporter gene GFP (Cre-GFP) into the dentate gyrus of $TrkB^{lox/lox}$ mice, we first confirmed that dendritic growth was also impaired by this approach in newborn neurons at 14 and 28 dpi as revealed by Sholl analysis (Fig. 5*A* and *B*). These morphological deficits were fully rescued by coinjection of retrovirus transducing functional TrkB (TrkB-DsRed) (Fig. 5*C-F*) together with that transducing Cre (Fig. 5*G* and *H*). When hippocampal sections stained with antibodies against GFP and DsRed were examined, single- and double-labeled neurons intermingled in the same sections disclosed a rather distinct dendritic complexity. Cells expressing GFP alone showed less complex dendritic arbors than

cells expressing only DsRed or cells expressing both GFP and DsRed, indicating that dendritogenesis was rescued by TrkB. Notably, dendrite growth could not be restored when catalytically inactive TrkB (TrkB FFF-DsRed; Fig. 5*C-F*) was used for rescue. Taken together these data indicate that there is indeed a regulation of dendritic arbor complexity by TrkB kinase activity specifically acting in neurons born in the adult dentate gyrus of the hippocampus.

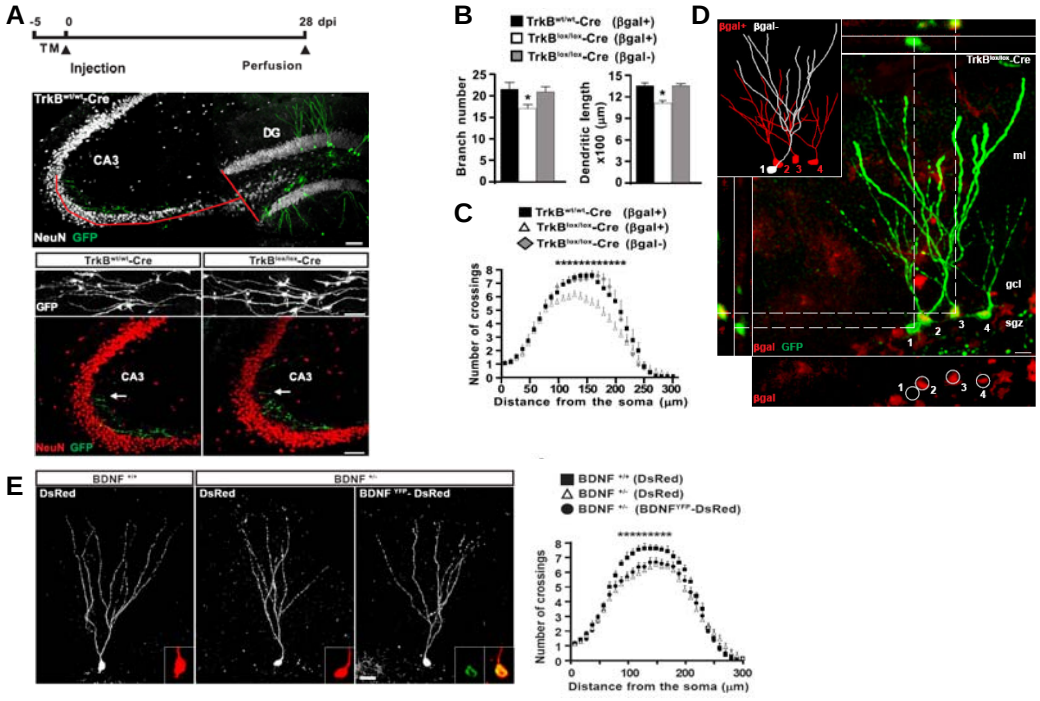

Figure 4*. TrkB is required for dendritic arborisation but not axonal growth in adult-born neurons. (*A*)** Schematic diagram showing the experimental paradigm used for retrovirus injection into tamoxifen-induced TrkB$^{lox/lox}$-Cre R26R and control mice. Viral injections were performed on the last day of tamoxifen treatment (0 dpi) and mice perfused 28 dpi. The left panel depicts GFP-transduced neurons (green) projecting axons to the CA3 region of the hippocampus. GFP immunoreactivity was superimposed on that of NeuN (gray). Axons were traced (red line) and scored. Bar, 50 µm. Panels on the right show high magnifications of the CA3 region. Arrows indicate the extreme axonal margins. Bar, 50 µm. Upper panels show the morphology of immunoreactive axons Bar, 10 µm. **(*B*)** Histograms show the total number of branches and the dendritic length of reporter positive (βgal+) or -negative (βgal-) cells virally transduced with GFP (*n*=20 neurons; 3 animals per genotype) (**, p<0.05). **(*C*)** Graph depicts Sholl analysis of the dendritic arbors in the same neurons as in *B* (*n*=20 neurons; 3 animals per genotype) (*****, p<0.05). **(*D*)** Representative confocal images depicting the dendritic morphology of reporter-positive (2–4; βgal+) or -negative (1; βgal-) cells transduced with GFP expressing retrovirus in TrkB$^{lox/lox}$-Cre R26R mice. Inset shows two-dimensional projection of tridimensional reconstruction of the cells Bar, 10 µm. **(*E*)** Regulation of dendritogenesis in newborn neurons by BDNF. Representative confocal pictures showing newborn neurons of wild type (BDNF$^{+/+}$) and heterozygous (BDNF$^{+/-}$) BDNF knockout mice upon injection of a retrovirus transducing DsRed or BDNF^{YFP}-DsRed. Graph on the right depicts the Sholl analysis of the dendritic arbor in transduced cells 28 dpi (n=20 cells; 2 animals per experimental group) (*p<0.05). Insets show DsRed (red) and BDNF^{YFP} (green) expression. Bar, 20 µm.

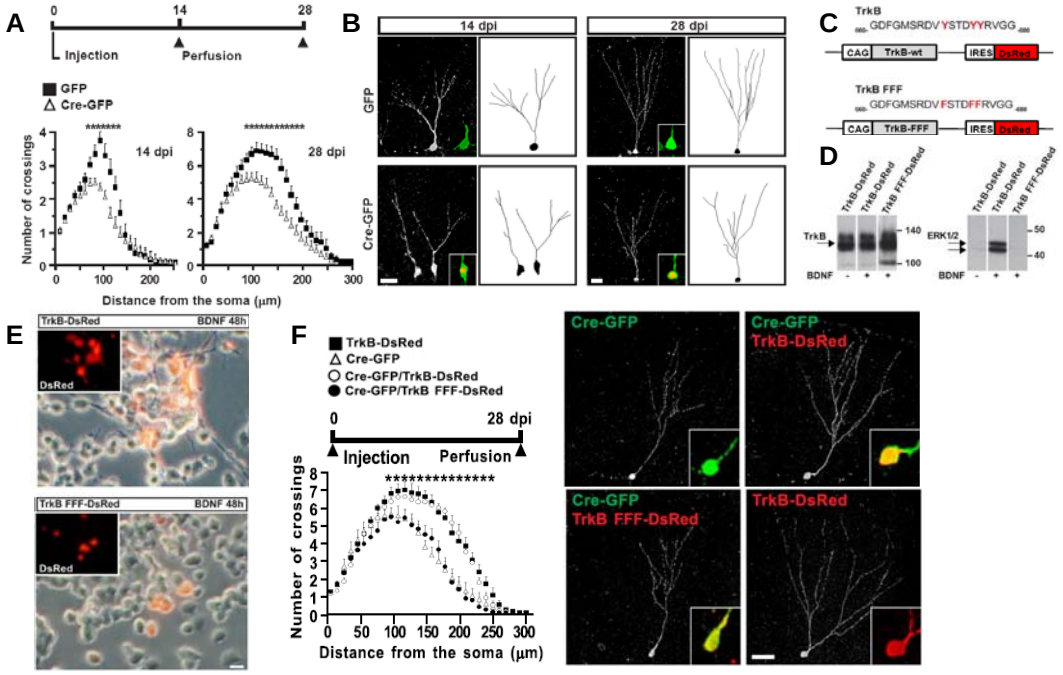

Figure 5. **Rescue of dendritic growth in TrkB-deficient newborn neurons. (*A*)** Schematic diagram showing the experimental paradigm used for retrovirus injection in $TrkB^{lox/lox}$ mice. Mice were injected with retrovirus transducing Cre-GFP or GFP alone and perfused 14 and 28 dpi. Graphs depict Sholl analysis of the dendritic arbor of transduced cells (n=20; 3 animals) (*p<0.05). **(*B*)** Representative confocal images and relative two dimensional projections of cells tranduced as in *A*. Insets show GFP (green) and Cre (red) expression. Bar, 20 μm. **(*C*)** Schematic diagram showing the tyrosines Y670, Y674, and Y675 that were mutated into phenylalanine (F) amino acids to generate the kinase-deficient TrkB FFF. Wild-type and mutated receptors were used to generate TrkB-DsRed and TrkB FFF-DsRed retrovirus, respectively, as symbolized on the bottom. **(*D*)** TrkB and TrkB FFF expression evaluated by Western blot in virally infected HEK293T cells. After infection, HEK293T cells were treated with BDNF for 15 min. Western blots show TrkB expression and receptor-mediated downstream signal transduction by using α-Trk and α-P-p42/44. p42/44 phosphorylation was increased in TrkB-, but not TrkB FFF-transduced cells following BDNF stimulation. **(*E*)** BDNF-mediated differentiation of PC12 cells transduced with TrkB-DsRed or TrkB FFF-DsRed retrovirus. Cells were subsequently treated with BDNF (48 h) for stimulating TrkB-mediated neurite outgrowth. Bar, 30 μm. **(*F*)** Schematic diagram showing the experimental paradigm. Graph depicts Sholl analysis of the dendritic arbor of cells single transduced (Cre or TrkB) or cotransduced (Cre/TrkB or Cre/TrkB FFF) with the retrovirus (*n*=10; 3 animals for each experimental group) (*, p<0.05). Representative confocal images of transduced cells are presented. Insets show the expression of the reporter marker GFP (green) and/or DsRed (red). Bar, 20 μm.

2.4.3 Spine growth

Injection of an improved retroviral vector (Zhao et al, 2006) in tamoxifen-induced control mice resulted in a persistent expression of GFP and strong fluorescence intensity of the dendritic segments at 28 dpi (Fig. 6*A*). This permitted us to visualize dendritic spines of rather diverse shapes and morphology, most of which appeared to be thin spines with small heads. Consistent with findings in wild-type mice (Zhao et al, 2006), total spine density was high and few spines with mushroom morphology were detected at this stage of development. However, spine density was significantly reduced upon TrkB deletion in newborn neurons of the same age. As an internal reference, we analyzed spines of the small fraction of βgal- neurons in these mice, showing that they possess a similar high density of spines to those in control littermates. Moreover, to assess whether spines could form excitatory and inhibitory synaptic contacts, we performed immunohistochemistry using glutamatergic (vGlut1) and GABAergic (vGAT) synaptic markers, respectively. Immunoreactivity for vGlut1 and vGAT was observed in both $TrkB^{lox/lox}$-cre and control mice, and some of these immunoreactive dots were opposed to GFP+ spines, thereby suggesting synapse formation (Fig. 6*B*).

2.4.4 Synapse formation

To assess directly whether spines could still form axo/dendritic synapses after TrkB deletion, we examined the architecture of the synapses of newborn neurons at the ultrastructural level using photoconversion of GFP in hippocampal sections from $TrkB^{lox/lox}$-Cre Z/EG mice 28 dptm followed by electron microscopy (Grabenbauer at al, 2005). This process converts GFP fluorescence into electron dense 3,3'-diaminobenzidine precipitates, allowing specific localization of the synaptic contacts. We focused on two hallmarks of mature synapses, the appearance of synaptic vesicles at presynaptic sites and the postsynaptic density. We observed that there are synapses formed by both TrkB-deficient and control newborn neurons, and their mature morphology matched that of reference synapses in the same preparations (Fig. 6*C*). Thus, TrkB-deficient neurons maintained the ability to form mature synaptic contacts.

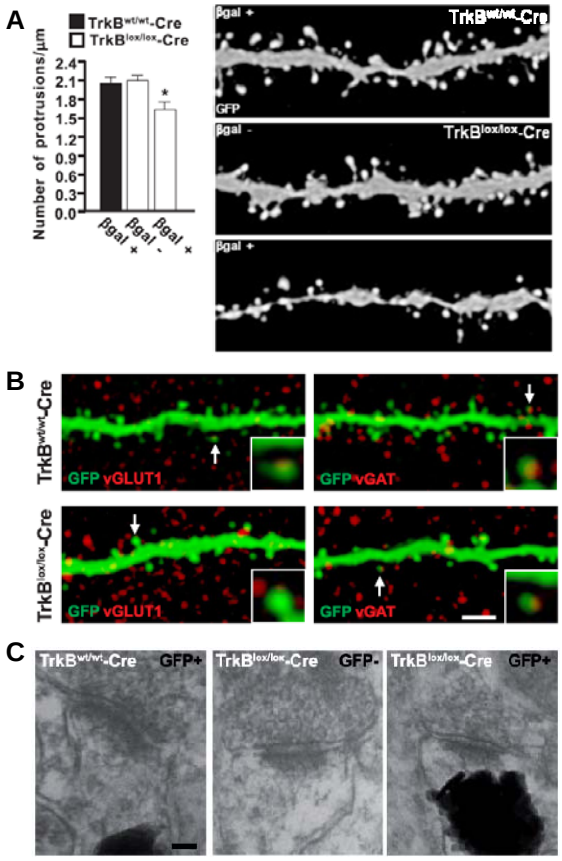

Figure 6. **Spine density is regulated by TrkB in adult-born neurons. (*A*)** Graphs depict the quantification of protrusions in dendritic segments of newborn neurons transduced with retrovirus expressing GFP in tamoxifen-induced TrkB$^{lox/lox}$-Cre R26R (*n*=24 dendritic segments; 18 βgal+; 11 βgal-; 3 animals) and control mice (*n*=60 dendritic segments; 26 βgal+; 3 animals) mice. The density of protrusions is expressed as number of protrusions per micrometer of dendritic length (*****, $p<0.01$). On the right, representative images show spine morphology in reporter-positive (βgal+) or -negative (βgal-) cells 28 dpi Bar, 2 µm. **(*B*)** Representative images show co-labeling of GFP with vGlut1 and vGAT in the medial molecular layer of the dentate gyrus. Immunoreactivity for vGlut1 and vGAT was observed in both TrkB$^{lox/lox}$-cre and control mice, and some of these immunoreactive dots were opposed to GFP-positive spines (arrows), thereby identifying synaptic contacts. Insets show threefold magnification of synaptic contacts. Bar, 2 µm. **(*C*)** Representative electron micrographs show synaptic contacts of newborn neurons in tamoxifen-induced TrkB$^{lox/lox}$-Cre Z/EG and control mice. Reporter-positive cells (GFP+) show GFP fluorescence as photoconverted electron-dense signals at postsynaptic sites. A synapse from a reporter-negative cell (GFP-) is shown as a reference. Bar, 50 nm.

2.4.5 Specific TrkB signaling pathways differently contribute to dendritic and spine growth

Overall, the data reported so far suggest that the reduced complexity of the dendritic arbor and spines, rather than synaptic contact *per se*, are morphological features regulated by TrkB in adult-born neurons. In order to assess the contribution of single tyrosine-dependent signalling pathways activated by TrkB to newborn neurons differentiation, we used different viral vectors specifically mutated in the tyrosines responsible for either Shc (TrkB^{Shc}-DsRed) or PLCγ (TrkB$^{PLC\gamma}$-DsRed) docking (Fig. 7*A*). Viruses were injected together with Cre-GFP retrovirus into the dentate gyrus of TrkB$^{lox/lox}$ mice. Consequently, in co-trasduced neurons endogenous TrkB was genetically deleted by the effect of Cre expression, while TrkB mutants were "de novo" expressed. Surprisingly, we observed that deletion of Shc-mediated pathway led to impaired dendritic arborization but comparable spine density to control neurons. Conversely, by mutating the PLCγ-dependent pathway, newborn neurons showed regular dendritic arbors but reduced spine density (Fig. 7*B* and *C*). Thus, these two signaling pathways are responsible for indipent dendritic morphological features.

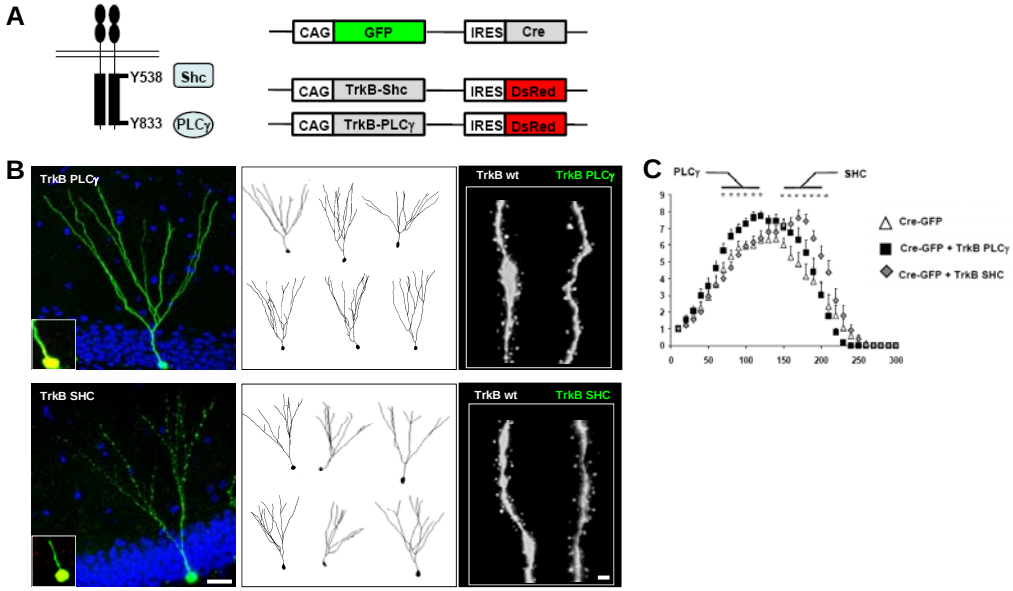

Figure 7. **Dendritic growth and spine density are regulated by distinct signaling pathways of TrkB. (*A*)** Schematic representation of the tyrosines located in the intracellular domain of TrkB and responsible for the activation of Shc- and PlCγ-signaling pathways. On the right, the design of the retroviral vectors ($TrkB^{Shc}$-DsRed and $TrkB^{PLCγ}$-DsRed) used for these experiments are shown. **(*B*)** Representative confocal images of cells double transduced with Cre-GFP and one of the two mutated isoforms of TrkB. Insets show the expression of the reporter markers GFP (green) and DsRed (red). Bar, 30 μm. Several examples of reconstructed traces for each TrkB isoform (TrkB PlCγ or TrkB Shc) are indicated. On the right, spines of representative dendritic segments in neurons transduced with different TrkB isoforms are shown. Bar, 2 μm. **(*C*)** Graph depicts Sholl analysis of the dendritic arbor of cells single transduced (Cre-GFP) or co-transduced with the TrkB-expressing viruses mutated either for the PlCγ (Cre-GFP + TrkB PlCγ) or the Shc (Cre-GFP + TrkB Shc) pathway (n=10; 3 animals for each experimental group) (*****, $p<0.05$).

2.5 Deletion of TrkB affects neurogenesis-dependent LTP in the dentate gyrus

Previous studies had indicated an important role for the endogenous BNDF/TrkB system in long-term plasticity, such as long-term potentiation (LTP) within the hippocampus. However, the contribution of TrkB on the LTP elicited in adult generated neurons could not be assessed by the previous approaches. As new neurons were shown to exhibit a small but stable form of LTP (Snyder et al, 2001; Saxe et al, 2006), which was distinguishable from that of the existing mature neurons in being insensitive to GABAergic inhibition and specific for the activation of the NMDA receptors subunit NR2B, we investigated whether this was adversely affected in $TrkB^{lox/lox}$-Cre vs. control mice. Slices derived from these mice were used for extracellular recordings between 28 and 42 dptm. Specifically, stimulation of medial perforant path (MPP) fibers evoked field excitatory postsynaptic potentials (fEPSPs), which were recorded by placing the extracellular recording electrode in the medial molecular layer of the upper blade of the dentate gyrus (Fig. 8*A*). The synaptic transmission was evaluated by testing input-output responses and paired-pulse depression in the dentate gyrus (Fig. 8*C*). One hundred-hertz stimulation elicited LTP that was stable during the recording time (>90 min) in slices from control mice and was prevented by pretreating slices with the NR2B inhibitor ifenprodil (3 μM) (Fig. 8*A*). On the contrary, slices from $TrkB^{lox/lox}$-Cre mice displayed a potentiation that lasted for only 30-40 min after stimulation, before returning to baseline (Fig. 8*A*). To confirm that the short-term potentiation was specifically attributable to TrkB-deficient newborn neurons, experiments were performed in the presence of the GABA receptor blocker bicuculline (20 μM), which unmasks the synaptic potentiation of granule neurons (Snyder at al, 2001; Saxe et al, 2006). Under this experimental condition, 100-Hz stimulation induced a large and persistent potentiation that was indistinguishable in slices from $TrkB^{lox/lox}$-Cre and control mice (Fig. 8*B*). Moreover, LTP was normal in the Schaffer/CA1 connections (data not shown), a region devoid of neurogenesis. Thus, targeted deletion of TrkB in newborn neurons causes an impairment in the late-phase of the neurogenesis-dependent form

of LTP without altering the synaptic plasticity of mature granule neurons in the same subfield.

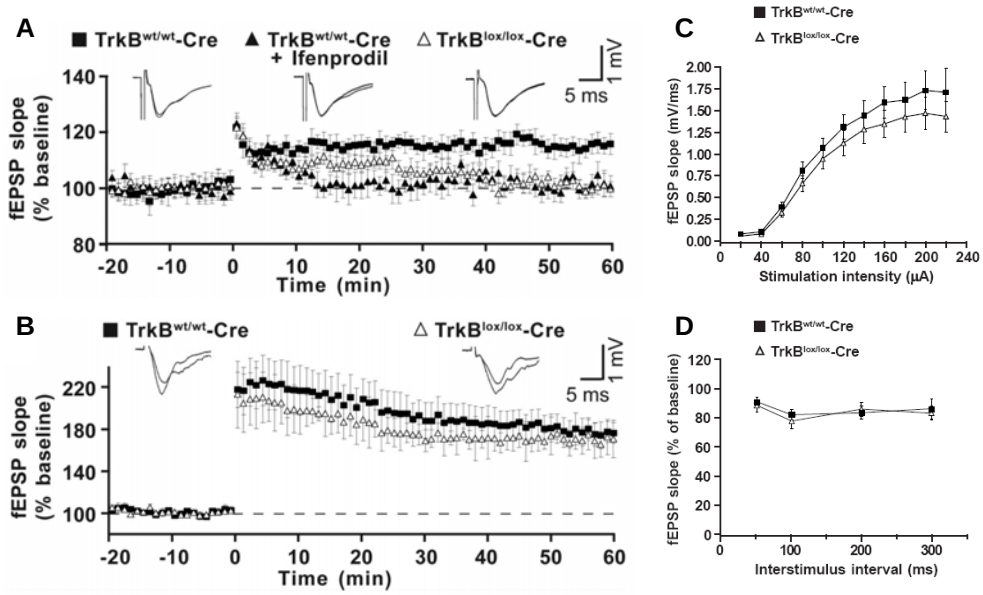

Figure 8. **TrkB expression in newborn neurons is required for neurogenesis-dependent LTP. (*A*)** LTP evoked in tamoxifen-induced TrkB$^{lox/lox}$-Cre and control mice. Experiments were conducted in hippocampal slices of TrkB$^{wt/wt}$-Cre mice in the absence (*n*=8 slices, 4 animals) or presence (*n*=6 slices, 2 animals) of ifenprodil (3 µM) and in slices of TrkB$^{lox/lox}$-Cre mice (*n*=7 slices, 3 animals). Each point in the graph shows the average fEPSP slope elicited in response to a test stimulus before (-20 - 0 min) and after (0 - 60 min) tetanic stimulation of the MPP. Representative fEPSP traces recorded before (-5 min) and after (60 min) tetanus are shown on the top. **(*B*)** LTP evoked as in *A* in the presence of bicuculline (20 µM) (*n* =4 slices, 4 animals). Synaptic transmission was evaluated by testing input–output responses **(*C*)** and paired-pulse depression (*D*) in the dentate gyrus of tamoxifen-induced TrkB$^{lox/lox}$-Cre and control mice.

2.6 Deficits in neurogenesis correlated with anxiety-like behavior

While the functions of newborn neurons in the adult are largely elusive, there is increasing evidence that adult neurogenesis (Sahay et al, 2007) and BDNF expression (Martinowich et al, 2007) in the dentate gyrus are involved in mood regulation. Our genetic approach now offered us the possibility to examine the effect of TrkB deletion on anxiety-like behavior specifically in recently generated neurons. We first focused on the open-field behavioral test, a well established paradigm used to study anxiety. We observed that $TrkB^{lox/lox}$-Cre mice between 28 and 42 dptm exhibited decreased spontaneous activity in the open-field arena compared with control littermates (Fig. 9*A* and *B*). While the distance traveled was comparable in these mice, TrkB-deficient mice entered the center areas of the arena less frequently and spent less time there than controls. Moreover, in the periphery (including the corners) the number of entries was reduced but the time spent was significantly increased. To further confirm the defects in exploratory behavior, mice were examined in the elevated plus maze test (Fig. 9*C* and *D*). Mice lacking TrkB specifically in the newborn neurons showed a significant decrease in the percentage of entries and time spent in the open arms vs. control littermates. The number of entries was comparable in these mice, consistent with the absence of any general activity defects. When the test was performed before TrkB-deficient newborn neurons had acquired morphological maturation, between 7 and 12 dptm, no differences in exploratory behavior were found between knockout and control mice (data not shown), indicating that alteration in anxiety-like behavior by TrkB does not take place before the morphological integration of adult-born neurons. Since neurogenesis has also been linked to spatial learning (Zhao et al, 2008), we tested whether this could be true in our experimental model where the integration of newborn neurons is specifically impaired. To this aim, we investigated the behavior of our mice in the Morris water maze test. During phases of the training period $TrkB^{lox/lox}$-Cre mice and control littermates were able to learn and memorize in parallel with equal efficiency (Fig. 10*A*). They initially located a visible platform (day 1) and further learned to locate the same platform hidden beneath the water surface in a constant location during the following phases (days 2–4). Latency to find

the platform, mean velocity, and total distance moved were statistically indistinguishable between mice. On day 5, the probe test disclosed again comparable parameters (Fig. 10*B*), with mice of both experimental groups spending similar amounts of time in the area were the platform was previously located, indicating that the spatial memory in mice lacking TrkB specifically in newborn neurons was not altered.

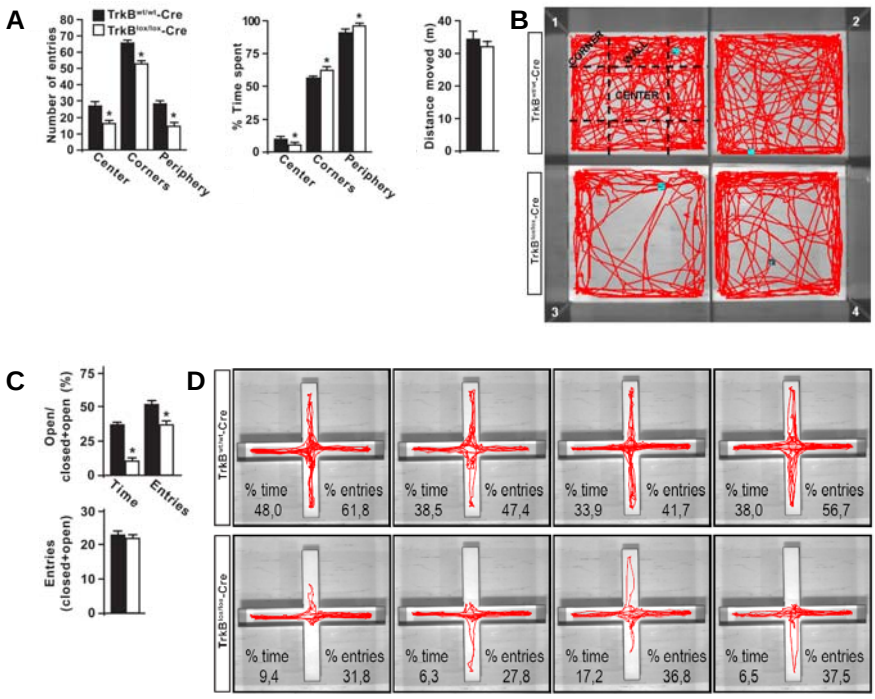

Figure 9. **Deletion of TrkB in newborn neurons affects exploratory activity in mice exposed to a novel environment. (*A*)** Exploratory behavior of tamoxifen-induced TrkB$^{lox/lox}$-Cre and control mice in the open-field test. Histograms show the number of entries and the percentage of time spent in the center, corner, or the entire periphery of the arena (n=20) (*****, P<0.05). The total distance moved is shown in the right panel. **(*B*)** Digital tracking of mice exposed to the open-field behavioral test. In red are depicted representative traces of mice pattern activity resulting from video tracking. Each panel is representative of individual mice activity. **(*C*)** Exploratory behavior in the elevated plus maze test. Histograms show the proportion of entries and time spent in the open arms (n=20) (*****, P<0.05). The total number of entries in the four arms is shown in the lower panel. **(*D*)** Digital tracking of mice exposed to the elevated plus maze test. Representative traces of mice pattern activity are shown as in *B*.

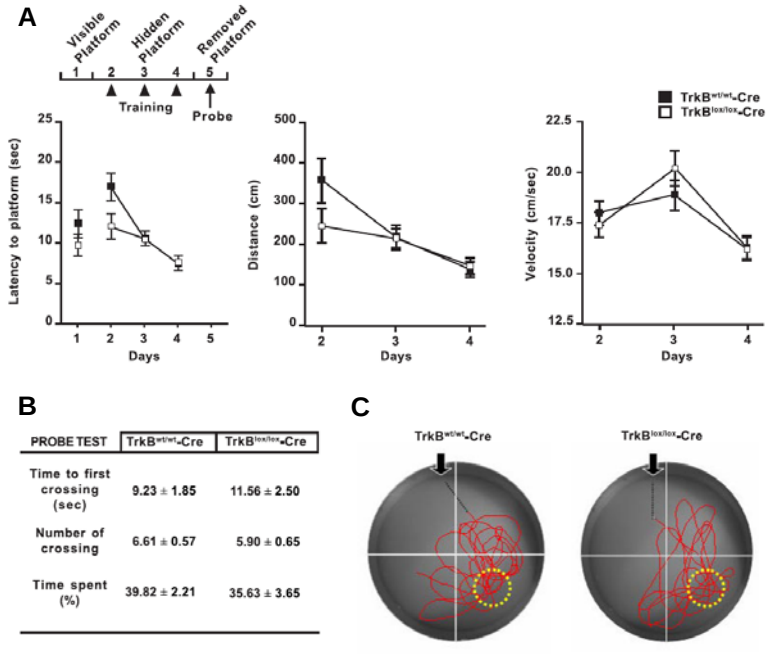

Figure 10. **Deletion of TrkB in newborn neurons does not alter spatial learning. (*A*)** Mice were subjected to the Morris water maze test between 28 and 42 dptm. The protocol used for the test is illustrated on the top left. On the graphs are reported the latency to find the hidden platform, the total distance moved and the mean velocity of TrkB$^{lox/lox}$-Cre and control mice during the training period (*n*=12). **(*B*)** On day 5, mice were subjected to a probe trial; the values (time and crossings) refer to a circular zone **(*C*)** around the place where the former platform was located (yellow annulus). Digital tracking of mice exposed to the Morris water maze test is shown in ***C***. In red are depicted representative traces of mice pattern activity resulting from video tracking.

2.7 Discussion

2.7.1 Impaired development of synaptic connections affects newborn neurons integration and survival

The first observation of the present study is that the survival of newborn neurons in the adult dentate gyrus depends critically on the activation of TrkB full-length receptor. The TrkB-dependent decision regarding life or death in these newborn neurons takes place right at the transition point where they mature from a Dcx-positive to a NeuN-positive stage, after 4 weeks of age. Before newborn neurons start to die, they exhibit a drastic reduction in dendritic complexity and spine density compared to wild-type newborn neurons, indicating that this receptor is required for the integration of adult-born neurons. Both the failure to become integrated and subsequent dying, and the loss of TrkB signaling lead to impaired LTP that has been shown to be specific for these young neurons (Snyder et al., 2001; Saxe et al., 2006). Finally, mice lacking a functional TrkB in the restricted population of newborn neurons show increased anxiety-like behavior. These data suggest that these neurons play a critical role in regulating the anxiety state of the animal.

As in development, the adult nervous system generates an excess number of new neurons but only a restricted population of the original pool survives (Lledo et al., 2006; Ninkovic and Götz, 2007). While the regulation of neuronal survival during development depends upon the supply of neurotrophic factors (Poo, 2001), the number of surviving neurons in the adult brain is thought to depend upon functional integration into the existing network, which, in turn has been suggested to be experience-dependent (Lledo et al., 2006). Here we found that, while the selective loss of NeuN positive newborn neurons is manifest only after 4 weeks post recombination, TrkB-deficient newborn neurons start to exhibit the first signs of decreased dendritic arborisation by 2 weeks. Noticeably, a similar reduction in dendritic complexity has been shown with knock down of the Na-K-2Cl co-transporter NKCC1 (Ge et al., 2006). This manipulation affects the chloride gradient in newborn neurons, thereby converting GABA prematurely into an inhibitory

transmitter on these neurons. The drastic loss of dendritic complexity in that study was also accompanied by a delay in synaptic innervation, both of GABA and glutamatergic inputs. The fact that TrkB deficient newborn neurons exhibit a marked reduction in the density of dendritic spines suggests that loss of this neurotrophin receptor is also accompanied by a loss of glutamatergic synapses at 4 weeks of age. Both dendritic morphology and synapse density suggest that there may be a functional interdependence between GABA and TrkB signaling in immature neurons. Loss of functional synaptic inputs may indeed be the cause for the subsequent cell death. Tashiro et al. (2006) found that specific deletion of NMDA receptors in newborn neurons drastically shortens the survival of these cells beginning from about week 3 and continuing to week 6. Despite the fact that no apparent deficits in dendritic morphology were reported in that study, one may speculate that the cell death in TrkB-deficient newborn neurons is not a direct consequence of the faulty morphological development but rather due to impaired functional synaptic input to these cells. Currently it is impossible to discern whether the deficit in dendritic arborisation is a consequence of faulty synaptic input or, conversely, the deficit in synaptic input is due to faulty dendritic arborisation. An interesting observation in the Tashiro study was that the reduced survival of immature neurons produced through loss of NMDA receptors could be rescued by pharmacological blockade of NMDA receptors in the dentate gyrus. This is taken as evidence for NMDA receptor activation mediating competitive selection among newborn neurons. Our observation that deletion of TrkB in the majority of newborn neurons did not prevent the effect on dendritic morphology and survival suggests that selective activation of TrkB is not involved in the competitive action through activation of the NMDA receptor.

While we cannot exclude that some aspects of axonal ramification also are affected in the absence of TrkB, we observed a normal development of the axonal projection to the CA3 region. This would suggest that the maturation of the dendritic and axonal compartments is differentially affected by the loss of TrkB and that the processes underlying the development of each compartment are not tightly interwoven. Thus, one interesting finding in our study is that the survival of newborn

neurons is primarily dependent upon the input received by these neurons rather than the output generated by them.

2.7.2 Impact of newborn neurons on the network activity specifically influences the emotional state

Our findings of impaired synaptic plasticity during postnatal 4 to 6 weeks of newborn neurons are reminiscent of the critical time period in which they show enhanced synaptic plasticity (Ge et al. 2007). Synaptic potentiation during this period depends on the activation of an NMDA receptor containing the NR2B subunit that is selectively expressed in these cells, but absent in mature neurons. Interestingly, LTP mediated by this NMDA receptor can be elicited in the absence of GABA-A receptor antagonists (Snyder et al., 2001; Saxe et al., 2006) suggesting that this LTP is exclusively localized to synapses on newborn neurons. Consistent with this interpretation is the fact that LTP induced in the absence of GABA-A antagonists is abrogated upon ablation of neurogenesis, for instance by irradiation (Wang et al., 2000; Snyder et al., 2001; Saxe et al., 2006). The present study showed that while an ifenprodil-sensitive LTP can be induced in wild-type mice, LTP is drastically impaired in mice in which the vast majority of newborn neurons lack TrkB. While an early, albeit reduced, LTP could be observed, the late-phase was totally abolished. The slight reduction in the early-phase of LTP may already reflect the reduced number of surviving neurons, while the lack of a late-phase of LTP is strikingly similar to the effect of the loss of TrkB or its ligand BDNF at the Schaffer collateral synapses (Korte et al., 1995). The lack of a long-term LTP may ultimately be the cause for the reduced number of synapses since these may not undergo activity-dependent stabilization. However, currently we cannot rule out that the deficit in LTP is a secondary consequence of the morphological maturation deficit. In any case the apparent deficit in synaptic long-term plasticity is likely to have an important bearing on the participation of newborn neurons in functional network activity. It was recently proposed that newborn neurons between 4 and 6 weeks are preferentially recruited in the context of exposure of mice to novel environments

(Kee et al., 2007), an effect thought to be due to new neurons' enhanced synaptic plasticity and excitability (Schmidt-Hieber et al., 2004; Ge et al., 2007).

The present study shows for the first time that mice lacking functional full-length TrkB specifically in the newborn neuron population (4 to 6 weeks after tamoxifen treatment) exhibited a markedly enhanced anxiety-like behavior as evidenced by their decreased explorative activity in the open field and elevated plus maze tests. Consistent with our results a recent study (Chen et al., 2006) demonstrated that mice expressing a BDNF variant (Val66Met) which shows an impairment in activity-dependent secretion of BDNF exhibit enhanced anxiety-like behavior. Remarkably, the behavioral phenotype correlated with a poor dendritic arborisation, highly reminiscent of the dendritic phenotype observed here. However, this study could not determine the possible contribution of adult-generated neurons to this phenotype. Here, we show that deletion of TrkB in newborn neurons is sufficient to cause an enhanced anxiety-like behavior, suggesting that the mood state may be particularly sensitive to the functional recruitment of newborn neurons. Intriguingly, a recent publication reported that the ablation of hippocampal neurogenesis does not result in anxietylike behavior (Saxe et al., 2006), so that the phenotype we observed may be due to an inappropriate functional integration of the surviving neurons rather than the death of the others. This interpretation supports the current idea that both neurogenesis (Sahay and Hen, 2007; Castrèn et al., 2007) and BDNF (Martinowitch et al., 2007) themselves are not etiological factors for anxiety, but rather, contribute indirectly to the activity of the hippocampal network that is involved in the emotional state. Hence, deficits in hippocampal circuitry have been implicated to influence the activity of structures receiving input from the hippocampus (i.e. prefrontal cortex, amygdala and nucleus accumbens) and associated with mood behavior (Lisman and Grace, 2005; Moser and Moser, 1998). In addition, regulation of the integration of newborn neurons into the existing hippocampal circuitry by BDNF could represent a molecular mechanism for plastic refinement of hippocampal network activity adapting to external inputs, which, in turn, may influence anxiety-like behavior. These inputs include physical exercise (Ernst et al., 2006), environmental enrichment (Nilsson et al., 1999) and common antidepressant drugs (Malberg et al., 2000), which

have been shown to influence mood-related behavior by regulating the rate of neurogenesis.

Anxiety and depression are often co-morbid and believed to share overlapping etiologies (Leonardo and Hen, 2006), a hypothesis supported by the common neuropharmacology of these disorders. However, in a paradigm often used to study depression-like behavior (tail suspension test), mice carrying TrkB deletion in adult-born neurons did not show apparent differences compared to wild-type mice, indicating that newborn neurons permit selected changes in adult brain function. In striking agreement with this specificity, we also observed that TrkB-deficient newborn neurons did not affect cognitive behavior in mice carrying the deletion. Hence, spatial learning and memory retention investigated in the Morris water maze test was normal in TrkB-deficient and control mice. How adult neurogenesis distinctly contributes to the regulation of anxiety leaving depression and some of the cognitive hippocampal functions unaffected remains an open question. At the network level, this specificity in behavior might result in selective activation of individual hippocampal circuits and extra-hippocampal brain areas, which, in turn, are regulated by TrkB. Thus, our data indicate that BDNF/TrkB system is a key regulator of adult-born neurons integration into hippocampal circuitry and that inhibition of TrkB signaling distinctly results in anxiety-like behaviour.

MATERIALS AND METHODS

1. Mice

$TrkB^{lox/lox}$ mice were provided by Rudiger Klein. $TrkB^{lox/lox}$-Cre mice were generated by crossing homozygous $TrkB^{lox/lox}$ mice with heterozygous GLAST-Cre::ERT2 R26R or Z/EG (Mori et al, 2006). $p75^{NTR}$ knockout mice were provided by Y.A. Barde. BDNF knockout mice were provided by M. Sendtner. The transgenic mice used for the present study were 2- to 3-months old and littermates were used as controls.

2. Viral Vectors

The Cre-internal ribosomal entry site (IRES)-GFPand IRES-GFP-encoding vectors were provided by K. Sawamoto. The murine Moloney leukemia virus (MoMulV)-based vector CAG-GFP (Zhao et al, 2006) was provided by F. H. Gage. We generated TrkB-IRES-DsRed, TrkB FFF-IRES-DsRed, $TrkB^{Shc}$-IRES-DsRed and $TrkB^{PLC\gamma}$-IRES-DsRed by cloning TrkB or kinase-mutated TrkB isoforms inside the IRES-DsRed-encoding vector provided by R. Jagasia. The final measured titer was about $5x10^8$ viral particles ml^{-1}.

3. Stereotaxic Surgery

Mice were anesthetized (100 mg ketamine, 10 mg xylazine in 10 ml saline) and retrovirus was infused into the dentate gyrus (spatial coordinates from Bregma: anteroposterior -2 mm, lateral ±1.6 mm, ventral 1.8 mm). Mice were then housed in standard cages and perfused 14 or 28 dpi. All experimental procedures were done in accordance with the Society for Neuroscience and European Union guidelines and were approved by our institutional animal care and utilization committee.

4. Immunocytochemistry and Immunohistochemistry

Slices or coverslips were permeabilized for 10 min in 0.5% Triton X-100 (Sigma) in PBS and incubated overnight in 3% BSA (Sigma) in PBS containing primary antibodies diluted 1:200, guinea pig anti-Dcx (Chemicon), rabbit or mouse anti-GFAP (Sigma), mouse anti-NeuN (Chemicon), rabbit anti-red fluorescent protein (Chemicon), rabbit anti-βgal (MP Biomedicals), mouse anti-Cre (Covance), anti-vGlut1 (Synaptic System), anti-vGAT (Synaptic System), anti-TrkB (Santa Cruz) and anti-TrkB (Chemicon), chicken anti-*pro*BDNF (Millipore), chicken anti-BDNF (Promega), goat anti-$p75^{NTR}$ (R&D Systems), rabbit anti-EEA1 (Abcam), rabbit anti-clathrin (Abcam), mouse anti-Vamp2 (Synaptic Systems), and mouse (Invitrogen) or chicken anti-GFP (Aves Laboratory) primary antibodies. Slices were incubated for 2 h at room temperature with secondary antibodies conjugated with FITC, Cy3, Cy5 (Chemicon), Alexa 488, 546, and 647 (Invitrogen), mounted in Aqua Poly/Mount (Polysciences, Inc.), and analyzed by confocal microscopy.Immunoreactivity was evaluated using a confocal laser-scanning microscope (Radiance 2000; Bio-Rad Laboratories) equipped with krypton–argon and red diode lasers and 20x/0.75, 60x/1.40, and 100x/1.40 oil objectives (Nikon). Alternatively, confocal analysis was performed by using a Leica SP5 system equipped with 10x, 40x, 63x and 100x objectives and long-lasting solid-state lasers with emission wavelengths of 405 nm, 488 nm, 532 nm, and 635 nm.

5. Quantitative analysis

Cell counting. Coronal brain sections (50 μm thick) of one-in-five series per hemisphere were selected for immunostaining. Three distinct areas (75,000 μm^2) of the dentate gyrus, including tip, upper, and lower blades were analyzed. Z-series stacks of 1 μm thick were taken with a 40x oil objective and immunoreactive cells were counted in each stack using the National Institutes of Health ImageJ software. *Morphometric analysis*. Coronal brain sections (130 μm thick) prepared from injected brains were selected for morphometric analysis. Z-series stacks 1.5 μm thick were taken with 40x and 60x oil objectives. The signal from immunoreactive dendrites was analyzed by deconvolution using the Huygens Professional 3.0

software (Scientific Volume Imaging, http://www.svi.nl) and 2D projection images of the 3D reconstructions were produced. Tracing and quantification of dendrites were obtained on 2D images using NeuronJ Plugin (http://imagescience.bigr.nl/meijering/software/neuronj). Only neurons showing intact dendritic arborization were analyzed. Sholl analysis was performed by Sholl Analysis Plugin (Ghosh Lab Website, http://biology.ucsd.edu/labs/ghosh/software/ ShollAnalysis.class) using a 10 μm interval between concentric circles. Immunoreactive axons were revealed by confocal acquisitions using 20x or 40x objectives; axonal length was scored as reported previously (Zhao et al, 2006). *Spine density*. Immunoreactive spines were visualized by confocal microscope using a 100x oil objective and digital 3x magnification. Z-series stacks were acquired with an interval of 0.3 μm between focal planes, processed by deconvolution and the number of spines was counted manually on the 2D projections using an additional digital zoom of 1.5x. The area of analysis was set on dendritic segments located in the medial region of the molecular layer of the upper blade at approximately the same distance from the cell body. After each acquisition, the same field (including the GCL) was reacquired with a 40x objective to confirm βgal expression in newborn neurons. Spine density was calculated by dividing the total number of spines by the length of the dendritic segments. *Signal co-localizations.* Image processing and volume rendering were performed using the ImageSpace software (Molecular Dynamics) running on an Indigo Workstation (Silicon Graphics).

6. Electron Microscopy.

TrkB-Cre mice induced for the expression of the recombination marker GFP were perfused with PBS followed by a solution of 4% paraformaldehyde in PBS. Photoconversion and electron microscopy were performed as previously reported (Grabenbauer et al, 2005). Briefly, sagittal slices 100 μm thick were incubated (1 h at 4°C) in 1 mg/ml 3,3'-diaminobenzidine and 50 nM potassium cyanide and irradiated under conventional epifluorescence using a 100-W mercury lamp and GFP fluorescence filter cube to induce photoconversion of 3,3'-diaminobenzidine

into an electron-dense residue. Slices were then postfixed in 2.5% glutaraldehyde in 0.1Mphosphate buffer for 30 min at 4°C followed by 1% OsO4 in the same buffer for 60 min at room temperature. In preembedding experiments, cultured astrocytes were treated with BDNF-YFP gold for 10 min, fixed in 2.5% glutaraldehyde (0.1 M phosphate buffer) for 30 min at 4°C, and postfixed in 1% OsO_4 for 60 min at room temperature. After dehydration, samples were embedded in Epon 812 and counterstained with uranyl acetate-lead citrate. Sections were examined with a Zeiss EM 109 electron microscope and images were captured with a charge-coupled device camera (DMX 1200F; Nikon). Digital images were collected and analyzed using Image Pro+ software (Media Cybernetics, Inc.). Analysis was performed on at least 200 micrographs disclosing intracellular structures containing gold particles. The vesicle diameters were measured referring to calibrated latex beads.

7. Slice preparation.

Hippocampal and cortical slices were prepared from 4-6 week old male Sprague-Dawley rats, $p75^{NTR}$ knockout mice or TrkB-Cre mice. The brain was removed and placed in cold (5° C) oxygenated (95% O_2 and 5% CO_2) artificial cerebrospinal fluid (ACSF) containing: NaCl 124.0 mM, KCl 4.4 mM, $CaCl_2$ 2.5 mM, $MgCl_2$ 1.3 mM, $NaHCO_3$ 26.2 mM, NaH_2PO_4 1.0 mM, glucose 10.0 mM, ascorbic acid 2.0 mM; pH 7.4. Hippocampal slices (350 μm thick) were prepared using an oscillating tissue slicer and transferred to a pre-incubation chamber containing oxygenated ACSF at room temperature.

8. Electrophysiology

Brain slices were preincubated for different times with 50 μM anisomycin (Tocris), 1 μg/ml TrkB-Fc (Regeneron Pharmaceuticals, Inc.), 200 nM K252a (Tocris), 50 μM MDC (Tocris), 20 μM D15 (Tocris), 70 μM LY294002 (Tocris), 20 μM bicuculline (Sigma), 100 ng/ml recombinant BDNF (Regeneron Pharmaceuticals, Inc.), Ifenprodil 3 μM (Tocris) and 100 nM plasmin (Sigma) Eventually, these drugs were maintained throughout the recording by a recirculation system. At least 60 min after

the slicing procedure, a single slice was transferred into a submersion recording chamber perfused (2 ml/min) with oxygenated ACSF at 30±0.2°C. For fEPSPs recorded in CA1 stratum radiatum a stimulating concentric bipolar electrode (40-80 KΩ, FHC) connected to a stimulus generator (AMPI) through a stimulus isolation unit was placed on Schaffer collaterals; for fEPSPs recorded in the middle molecular layer of dentate gyrus, the stimulating electrode was placed the medial perforanth path (Colino and Malenka, 1993); for fEPSPs recorded in layer II/III of perirhinal cortex, the stimulating electrode was placed nearby the recording pipette on the same layer for stimulating horizontal fibers. Field EPSPs were recorded with NaCl (2M)-filled glass pipettes (< 5 MΩ) connected to a DC current amplifier, digitized (10 KHz) and analyzed using Axoscope 8.0 software (Axon Instruments Inc.) or IGOR PRO software (Wavemetric). Input-output curves were obtained after 20 min of stable recording and the stimulation intensity that produced half of the maximal response was used for test pulses and tetanic stimulation. Baseline recordings were conducted with a frequency of one test stimulus (square pulses, 200 ms) every 20 s. Only slices showing fEPSPs of 1 mV in amplitude or higher were selected for experiments. For CA1 and cortical LTP, potentiation was induced by TBS stimulation, consisting of 12 bursts, each one formed by 4 pulses at 100 Hz, with an inter-burst interval of 200 ms. For dentate gyrus-LTP, potentiation was induced bya tetanic stimulation which consisted of four trains of 500 ms each, 100 Hz within the train, repeated every 20 s.

9. Biotinylation assay

Cultured cells were incubated with recombinant BDNF (100 ng/ml) for 60 min. After acid wash, cell-surface biotinylation of intact astrocytes was performed on ice using an immunolabeling kit (Pierce). Cells were then lysed and half of each sample was subjected to overnight precipitation using agarose-conjugated streptavidin (Sigma), which recognizes biotin-labeled proteins. The second half was subjected to overnight precipitation using WGA-agarose (Sigma), which recognizes glycoconjugate

proteins. The precipitates were analyzed by Western blot and aliquots of the cell lysates by ELISA.

10. Western blot

Immunoprecipitation and immunopurification products were separated by SDS-PAGE and transferred to nitrocellulose membranes (0.45 μm) using standard procedures. After blocking unspecific sites, the membranes were incubated overnight at 4°C with primary mouse α-TrkB (BD Transduction Laboratories), chicken α-BDNF (R&D Systems), rabbit and chicken α-*pro*BDNF (Millipore), mouse α-TrkB (BD Biosciences), rabbit α-$p75^{NTR}$ (Abcam), mouse α-Vamp2 (Synaptic Systems), and mouse α-Map2 (a gift from A. Matus, Friedrich Miescher Institut, Basel, Switzerland) primary antibodies.. Detection was performed after 60 min incubation with secondary antibodies conjugated to horseradish peroxidase (Pierce) and subsequent conversion with a chemiluminescent substrate (Pierce).

11. Cell cultures

Primary cultures of cortical astrocytes were prepared from postnatal day 1-2 Wistar rats and $p75^{NTR+/+}$ or $p75^{NTR-/-}$ mice (provided by Y.-A. Barde, Biozentrum, University of Basel, Basel, Switzerland) as previously described (McCarthy and de Vellis, 1980) and mantained in DMEM with 10% fetal bovine serum (GIBCO) at 37°C in 5% CO_2.

12. Production of BDNF-YFP

The cDNA coding for BDNF-YFP (provided by O. Griesbeck, Max Planck Institute of Neurobiology, Martinsried, Germany) was transfected into COS-7 cells cultured in reduced (5%) FBS using a conventional diethylaminoethyl-dextran procedure. The supernatant containing the secreted proteins was collected and concentrated to obtain standard solutions of BDNF-YFP ranging from 10 to 100 pg/ml.

13. Characterization of BDNF the immunocomplexes *pro*BDNF-QD

QD-565 surfaces immobilized with α-rabbit antibodies (Invitrogen) were used to passively bind rabbit α-*pro*BDNF (Millipore). According to the manufacturer, a single QD-565 shows the potential to be bio-conjugated to <10 antibody molecules; thus, the desired degree of immunocoupling was set by adjusting the mixing stoichiometry between QDs and α-*pro*BDNF to 1:10. Incubation was performed for 10 min in a neutral buffer at 37°C. The final immunocomplex was obtained in a second step by incubating the QD/α-*pro*BDNF mixture with 100 ng/ml BDNF (mix), which contains BDNF in both precursor and mature forms. The correct formation of the *pro*BDNF-QD immunocomplex was confirmed by immunocytochemistry. The intensity profile of *pro*BDNF-QD fluorescence was determined and compared with individual QDs as a reference. Although individual *pro*BDNF-QDs showed high fluorescent fluctuation (blinking), *pro*BDNF-QD clusters produced a larger variation in brightness but lower blinking. Confocal imaging revealed that 10 nM *pro*BDNF-QDs were sufficient to visualize individual dots internalized into cultured astrocytes transfected with p75-GFP or Lck-GFP (provided by H. Lickert, Helmholtz Zentrum Muenchen, Neuherberg, Germany) Higher concentrations (20-500 nM) increased QD clustering at the cell interspace and QDs decorated the surface of the cells, but internalization was strongly impaired.

14. BDNF-YFP gold

The immunocomplex was prepared by two-step coupling procedures in which BDNF-YFP (mix) was first coupled with α-GFP for 10 min and subsequently with a secondary antibody coupled with 5-nm gold particles.

15. Time-lapse TIRF imaging

Cortical astrocytes or vestibular Schwann cells growth on glass coverslip (number 0) were incubated with BDNF-YFP or acridine-orange, respectively, for 1-5 minutes and perfused at a rate of 0.1 ml/min in Hanks modified medium at room temperature.

Time-lapse imaging was conducted using an Olympus inverted microscope IX71 equipped with a 60x objective Plapon/TIRFM-SP1 oil immersion and diode solid state lasers (488 and 532 nm). During acquisition, the laser beam was tilted at a specific critical angle to obtain total internal reflection at the glass-cell interface according to Snell's law. The refractive indices for glass (n = 1.52 at 488 nm) and cells (n = 1.38) predict an evanescent field in which excitation of the fluorophores is restricted to a region less than 100 nm in thickness. We imaged YFP and acridine-orange fluorescence in sequential mode under evanescent field illumination. To prevent photo-bleaching of the sample, images were acquired for only 10-40 ms in 250 ms intervals. Light was filtered with a dual band FITC/TRIC filter set (Olympus). Fluorescence images were visualized using a CCD camera (FV2T, Olympus). Video images were analyzed with CellR software. Only when double fluorescence increased, spread and then declined, was the event counted as a flash.

16. Characteristics of the perfusion setup and release experiments

Stimulation of cell cultures was obtained by adding 50 μM glutamate, 50 μM AMPA, and 100 μM t-ACPD over a 5-min period. Treatment with specific receptor antagonists (50 μM CNQX and 500 μM AIDA) started 30 min before the beginning of the perfusion and was maintained throughout the collection period. Intoxication with TeNT started 12 h before the beginning of perfusion and was not maintained throughout the collection period. High frequency stimulation, consisting in bursts formed by 50 biphasic 10 ms square pulses, delivered at 50 Hz for 5 min with an interburst interval of 25 s, was performed as previously described (Balkowiec & Katz , 2000). The amount of BDNF in each fraction was determined by a two-site BDNF ELISA (Canossa et al., 1997). The amount of BDNF in each fraction was determined by ELISA and expressed in pg/ml. For statistical analysis the data are presented as the means of BDNF content in the fractions collected before (basal) and during the stimulations.

17. Purification of vesicles

Cultured cortical astrocytes were incubated with recombinant BDNF (100 ng/ml) on Petri dishes and harvested by scraping and re-suspended in homogenization buffer (10 mM HEPES–KOH pH 7.4, 250 mM sucrose, 1 mM Mg-actetate). The cells were homogenized using a cell cracker (European Molecular Biology Laboratory) and centrifuged at 1000 *g* for 10 min to prepare the post-nuclear supernatant. Vesicles were immunoisolated from the postnuclear supernatant with a-mouse Dynabeads (M-280) coated with mouse a-$p75^{NTR}$ (Sigma-Aldrich), mouse a-Vamp2 (Synaptic Systems), or mouse a-Map2 (a gift from A. Matus) antibodies according to the manufacturer's instructions. Bound vesicles were further analyzed by Western blot and ELISA and processed for electron microscopy.

18. Enzyme immunoassay (ELISA)

BDNF was quantified by using a two-site immunoassay (Canossa *et al*, 1997). Briefly, microtiter plates were coated with a mAb BDNF#1 in 0.05 sodium carbonate buffer (pH 9.7) and incubated overnight at 4°C. After washing with 0.05 M Tris-HCl (pH 7.0), 0.2 M NaCl 0.1%, Triton X-100 buffer and blocking with 1% BSA in washing buffer, standards (2–500 pg/ml) and samples were incubated overnight at 4°C. A third overnight incubation step with the mAb BDNF#9 conjugated to peroxidase. The assay was developed by using BM Blue peroxidase substrate (Boehringer Mannheim). The BDNF ELISA showed a sensitivity of 1–3 pg/ml of BDNF.

19. Open Field

Mice were placed in the experimental room 1 h before the test. Open field activity was measured in a square arena (50x50 cm). At the beginning of a session, mice were placed in the central part of the arena. We scored the number of entries into the center, corners, and periphery (corners plus walls) and the time spent in the same areas by video-tracking recording for 20 min. Experiments were carried out under white light between 09:00 and 15:00 h and activity was videotaped and scored by EthoVision software (Noldus, The Netherland).

20. Elevated Plus Maze

Mice were placed in the experimental room 1 h before the test. The apparatus consisted of two open arms, two enclosed arms of the same size (30x8 cm), and a central area (8x8 cm); placement was 50 cm above the floor. At the beginning of a session, mice were placed in the central part of the maze facing one of the open arms. The number of entries and the time spent in the open and close arms were recorded for 5 min. An entry was defined as the mice entering into an arm with all four paws. The test was run out between 09:00 and 15:00 and behavior was videotaped and scored by EthoVision software.

21. Statistical analysis

The results are presented as means ± SEM and the statistical significance was determined using the unpaired Student's *t*-test. Alternatively, data were analyzed using multiple comparison one-way ANOVA followed by Tukey's post hoc test.

REFERENCES

Aicardi G, Argilli E, Cappello S, Santi S, Riccio M, Thoenen H, Canossa M (2004) Induction of long-term potentiation and depression is reflected by corresponding changes in secretion of endogenous brain-derived neurotrophic factor. *Proc Natl Acad Sci USA* 101: 15788–15792.

Aimone J-B, Wiles J, Gage F-H (2006) Potential role for adult neurogenesis in the encoding of time in new memories. *Nat Neurosci* 9:723–727.

An JJ, Gharami K, Liao GY, Woo NH, Lau AG, Vanevski F, Torre ER, Jones KR, Feng Y, Lu B, and Xu B (2008) Distinct role of long 3' UTR BDNF mRNA in spine morphology and synaptic plasticity in hippocampal neurons. *Cell* 134: 175 – 187.

Balkowiec A, Katz DM (2000) Activity-dependent release of endogenous brain-derived neurotrophic factor from primary sensory neurons detected by ELISA in situ. *J Neurosci* 20: 7417–7423.

Barco A, Patterson S, Alarcon JM, Gromova P, Mata-Roig M, Morozov A, Kandel ER (2005) Gene expression profiling of facilitated L-LTP in VP16-CREB mice reveals that BDNF is critical for the maintenance of LTP and its synaptic capture. *Neuron* 48: 123–137.

Benraiss A, Chmielnicki E, Lerner K, Roh D, Goldman SA (2001) Adenoviral brain-derived neurotrophic factor induces both neostriatal and olfactory neuronal recruitment from endogenous progenitor cells in the adult forebrain. *J Neurosci* 21: 6718-31.

Bezzi P, V Gundersen, JL Galbete, G Seifert, C Steinhauser, E Pilati, A Volterra (2004) Astrocytes contain a vesicular compartment that is competent for regulated exocytosis of glutamate. *Nat Neurosci* 7 :613 – 620 .

Blochl A, Thoenen H (1995) Characterization of nerve growth factor (NGF) release from hippocampal neurons: evidence for a constitutive and an unconventional sodium-dependent regulated pathway. *Eur J Neurosci* 7: 1220–1228.

Bronfman FC, M Tcherpakov, TM Jovin, M Fainzilber (2003) Ligandinduced internalization of the p75 neurotrophin receptor: a slow route to the signaling endosome. *J Neurosci* 23 :3209 – 3220 .

Butowt R, von Bartheld CS (2001) Sorting of internalized neurotrophins into an endocytic transcytosis pathway via the Golgi system: ultrastructural analysis in retinal ganglion cells. *J Neurosci* 21: 8915–8930.

Butowt R, von Bartheld CS (2005) Anterograde axonal transport of BDNF and NT-3 by retinal ganglion cells: roles of neurotrophin receptors. *Mol Cell Neurosci* 29: 11–25.

Caleo M, Menna E, Chierzi E, Cenni MC, Maffei L (2000) Brainderived neurotrophic factor is an anterograde survival factor in the rat visual system. *Curr Biol* 5: 1155–1161.

Caleo M, Medini P, von Bartheld CS, Maffei L (2003) Provision of brain-derived neurotrophic factor via anterograde transport from the eye preserves the physiological responses of axotomized geniculate neurons. *J Neurosci* 23: 287–296.

Canossa M, Griesbeck O, Berninger B, Campana G, Kolbeck R, Thoenen H (1997) Neurotrophin release by neurotrophins: implications for activity-dependent neuronal plasticity. *Proc Natl Acad Sci USA* 94: 13279–13286.

Canossa M, Gartner A, Campana G, Inagaki N, Thoenen H (2001) Regulated secretion of neurotrophins by metabotropic glutamate group I (mGluRI) and Trk receptor activation is mediated via phospholipase C signalling pathways. *EMBO J* 20: 1640–1650.

Castrén E, Võikar V, Rantamäki T. (2007) Role of neurotrophic factors in depression. *Curr Opin Pharmacol* 7: 18-21.

Chao MV (2003) Neurotrophins and their receptors: a convergence point for many signalling pathways. *Nat Rev Neurosci* 4:299-309.

Chen G, Kolbeck R, Barde YA, Bonhoeffer T, Kossel A (1999) Relative contribution of endogenous neurotrophins in hippocampal long-term potentiation. *J Neurosci* 19: 7983–7990.

Chen WG, Chang Q, Lin Y, Meissner A, West AE, Griffith EC, Jaenisch R, Greenberg ME (2003) Derepression of BDNF transcription involves calcium-dependent phosphorylation of MeCP2. *Science* 31: 885–889.

Chen ZY, Patel PD, Sant G, Meng CX, Teng KK, Hempstead BL, Lee FS (2004) Variant brain-derived neurotrophic factor (BDNF) (Met66) alters the intracellular trafficking and activity-dependent secretion of wild-type BDNF in neurosecretory cells and cortical neurons. *J Neurosci* 24: 4401–4411.

Chiaramello S, Dalmasso G, Bezin L, Marcel D, Jourdan F, Peretto P, Fasolo A, De Marchis S (2007) BDNF/ TrkB interaction regulates migration of SVZ precursor cells via PI3-K and MAP-K signalling pathways. *Eur J Neurosci* 26: 1780-90.

Colino A, Malenka R-C (1993) Mechanisms underlying induction of long-term potentiation in rat medial and lateral perforant paths in vitro. *J Neurophysiol* 69:1150–1159.

Conner JM, Lauterborn JC, Yan Q, Gall CM, Varon S (1997) Distribution of brain-derived neurotrophic factor (BDNF) protein and mRNA in the normal adult rat CNS: evidence for anterograde axonal transport. *J Neurosci* 17: 2295–2313.

Danzer SC, McNamara JO (2004) Localization of brain-derived neurotrophic factor to distinct terminals of mossy fiber axons implies regulation of both excitation and feedforward inhibition of CA3 pyramidal cells. *J Neurosci* 2450:11346-55.

Doetsch F, Caillé I, Lim DA, García-Verdugo JM, Alvarez-Buylla A (1999) Subventricular zone astrocytes are neural stem cells in the adult mammalian brain. *Cell* 97:703-16.

Du J, Feng L, Yang F, Lu B (2000) Activity- and Ca(2+)-dependent modulation of surface expression of brain-derived neurotrophic factor receptors in hippocampal neurons. *J Cell Biol* 150: 1423–1434.

Du J, Feng L, Zaitsev E, Je HS, Liu XW, Lu B (2003) Regulation of TrkB receptor tyrosine kinase and its internalization by neuronal activity and Ca2+ influx. *J Cell Biol* 163: 385–395.

Egan MF, Kojima M, Callicott JH, Goldberg TE, Kolachana BS, Bertolino A, Zaitsev E, Gold B, Goldman D, Dean M, Lu B, Weinberger DR (2003) The BDNF val66met polymorphism affects activity-dependent secretion of BDNF and human memory and hippocampal function. *Cell* 112: 257–269.

Eriksson PS, Perfilieva E, Björk-Eriksson T, Alborn AM, Nordborg C, Peterson DA, Gage FH (1998) Neurogenesis in the adult human hippocampus. *Nat Med* 4:1313-7.

Ernfors, P, C Wetmore, L Olson, H Persson (1990) Identification of cells in rat brain and peripheral tissues expressing mRNA for members of the nerve growth factor family. *Neuron* 5: 511 – 526 .

Ernfors P, Van De Water T, Loring J, Jaenisch R (1995) Complementary roles of BDNF and NT-3 in vestibular and auditory development. *Neuron* 14:1153–1164.

Ernst C, Olson AK, Pinel JP, Lam RW, Christie BR (2006) Antidepressant effects of exercise: evidence for an adult-neurogenesis hypothesis? *J Psychiatry Neurosci* 31: 84-92.

Fayard B, S Loeffler, J Weis, E Vögelin, A Krüttgen (2005) The secreted brain-derived neurotrophic factor precursor proBDNF binds to TrkB and p75NTR but not to TrkA or TrkC. *J Neurosci Res* 80 :18 – 28 .

Ge S, Goh EL, Sailor KA, Kitabatake Y, Ming GL, Song H (2006) GABA regulates synaptic integration of newly generated neurons in the adult brain. *Nature* 439:589-593.

Ge S, Yang C-H, Hsu K-S, Ming G-L, Song H-A (2007) Critical period for enhanced synaptic plasticity in newly generated neurons of the adult brain. *Neuron* 54:559–566.

Grabenbauer M, Geerts WJ, Fernadez-Rodriguez J, Hoenger A, Koster AJ, Nilsson T (2005) Correlative microscopy and electron tomography of GFP through photooxidation. *Nat Methods* 2:857-62.

Hartmann M, Heumann R, Lessmann V (2001) Synaptic secretion of BDNF after high-frequency stimulation of glutamatergic synapses. *EMBO J* 20: 5887–5897.

Hastings N-B, Gould E (1999) Rapid extension of axons into the CA3 region by adult-generated granule cells. *J Comp Neurol* 413:146–154.

Kandel ER (2001) The molecular biology of memory storage: a dialogue between genes and synapses. *Science* 294: 1030–1038.

Kee N, Teixeira C-M, Wang A-H, Frankland P-W (2007) Preferential incorporation of adult-generated granule cells into spatial memory networks in the dentate gyrus. *Nat Neurosci* 10:355–362.

Kempermann G, Gast D, Kronenberg G, Yamaguchi M, Gage FH (2003) Early determination and long-term persistence of adult-generated new neurons in the hippocampus of mice. *Development* 130: 391-399.

Klein R, D Conway, LF Parada, M Barbacid (1990). The trkB tyrosine protein kinase gene codes for a second neurogenic receptor that lacks the catalytic kinase domain. *Cell* 61: 647 – 656.

Klein R, Smeyne RJ, Wurst W, Long LK, Auerbach BA, Joyner AL, Barbacid M (1993) Targeted disruption of the trkB neurotrophin receptor gene results in nervous system lesions and neonatal death. *Cell* 75:113-22.

Kohara K, Kitamura A, Morishima M, Tsumoto T (2001) Activitydependent transfer of brain-derived neurotrophic factor to postsynaptic neurons. *Science* 291: 2419–2423.

Korte M, Carroll P,Wolf E, Brem G, Thoenen H, Bonhoeffer T (1995) Hippocampal long-term potentiation is impaired in mice lacking brain-derived neurotrophic factor. *Proc Natl Acad Sci USA* 92: 8856–8860.

Korte M, Griesbeck O, Gravel C, Carroll P, Staiger V, Thoenen H, Bonhoeffer T (1996) Virus-mediated gene transfer into hippocampal CA1 region restores longterm potentiation in brainderived neurotrophic factor mutant mice. *Proc Natl Acad Sci USA* 29: 12547–12552.

Lee R, Kermani P, Teng KK, Hempstead BL (2001) Regulation of cell survival by secreted proneurotrophins. *Science* 294: 1945-1948.

Leonardo ED, Hen R (2006) Genetics of affective and anxiety disorders. *Annu Rev Psychol* 57:117-137.

Lessmann V, Gottmann K, Malcangio M (2003) Neurotrophin secretion: current facts and future prospects. *Prog Neurobiol* 69: 341–374.

Lisman JE, Grace AA (2005) The hippocampal-VTA loop: controlling the entry of information into long-term memory. *Neuron* 46:703–713.

Lledo P-M, Alonso M, Grubb M-S (2006) Adult neurogenesis and functional plasticity in neuronal circuits. *Nat Rev* 7:179–193.

Lou H, Kim SK, Zaitsev E, Snell CR, Lu B, Loh YP (2005) Sorting and activity-dependent secretion of BDNF require interaction of a specific motif with the sorting receptor carboxypeptidase E. *Neuron* 45:245-55.

Lu B (2004) Acute and long-term synaptic modulation by neurotrophins. *Prog Brain Res* 146: 137–150.

Lu B (2005) The yin and yang of neurotrophin action. *Nat Rev Neurosci* 6: 603 – 614.

Malberg JE, Eisch AJ, Nestler EJ, Duman RS (2000) Chronic antidepressant treatment increases neurogenesis in adult rat hippocampus. *J Neurosci* 20:9104-9110.

Markakis E-A, Gage F-H (1999) Adult-generated neurons in the dentate gyrus send axonal projections to field CA3 and are surrounded by synaptic vesicles. *J Comp Neurol* 406:449–460.

Martinowich K, Manji H, Lu B (2007) New insights into BDNF function in depression and anxiety. *Nat Neurosci* 10:1089–1093.

Matsumoto, T., S. Rauskolb , M. Polack, J. Klose, R. Kolbeck, M. Korte, and Y.A. Barde (2008) Biosynthesis and processing of endogenous BDNF: CNS neurons store and secrete BDNF, not proBDNF. *Nat Neurosci* 11: 131 – 133.

Maxfield FR, TE McGraw (2004) Endocytic recycling. *Nat Rev Mol CellBiol* 5 :121 – 132 .

McAllister AK, Katz LC, Lo DC (1999) Neurotrophins and synaptic plasticity. *Annu Rev Neurosci* 22: 295–318.

McAllister AK (2002) Spatial restricted actions of BDNF. *Neuron* 36: 549–550.

Minichiello L, Piehl F, Vazquez E, Schimmang T, Hokfelt T, Represa J, Klein R (1995) Differential effects of combined trk receptor mutations on dorsal root ganglion and inner ear sensoryneurons. *Development* 121: 4067–4075.

Minichiello L, Korte M, Wolfer D, Kühn R, Unsicker K, Cestari V, Rossi-Arnaud C, Lipp HP, Bonhoeffer T, Klein R (1999) Essential role for TrkB receptors in hippocampus-mediated learning. *Neuron* 24:401-14.

Montana V, EB Malarkey, C Verderio, M Matteoli, V Parpura (2006) Vesicular transmitter release from astrocytes. *Glia* 54 :700 – 715 .

Mori T, Tanaka K, Buffo A, Wurst W, Kühn R, Götz M (2006) Inducible gene deletion in astroglia and radial glia--a valuable tool for functional and lineage analysis. *Glia* 54:21-34.

Moser MB, Moser EI (1998) Functional differentiation in the hippocampus. *Hippocampus* 8: 608–619.

Mowla SJ, Pareek S, Farhadi HF, Petrecca K, Fawcett JP, Seidah NG, Morris SJ, Sossin WS, Murphy RA (1999) Differential sorting of nerve growth factor and brain-derived neurotrophic factor in hippocampal neurons. *J Neurosci* 19: 2069–2080.

Mowla SJ, Farhadi HF, Pareek S, Atwal JK, Morris SJ, Seidah NG, Murphy RA (2001) Biosynthesis and post-translational processing of the precursor to brain-derived neurotrophic factor. *J Biol Chem* 276: 12660–12666.

Nagappan G, Zaitsev E, Senatorov VV Jr, Yang J, Hempstead BL, Lu B (2009) Control of extracellular cleavage of ProBDNF by high frequency neuronal activity. *Proc Natl Acad Sci U S A* 106:1267-72.

Naumann T, E Casademunt, E Hollerbach, J Hofmann, G Dechant, M Frotscher, YA Barde (2002) Complete deletion of the neurotrophin receptor p75NTR leads to long-lasting increases in the number of basal forebrain cholinergic neurons. *J Neurosci* 22 :2409 – 2418 .

Nilsson M, Perfilieva E, Johansson U, Orwar,O, Eriksson PS (1999) Enriched environment increases neurogenesis in the adult rat dentate gyrus and improves spatial memory. *J Neurobiol* 39:569-578.

Ninkovic J, Götz M (2007) Signaling in adult neurogenesis: From stem cell niche to neuronal networks. *Curr Opin Neurobiol* 17:338–344.

Oh-Hashi K, Ito M, Tanaka T, Hirata Y, Kiuchi K (2009) Biosynthesis, processing, and secretion of glial cell line-derived neurotrophic factor in astroglial cells. *Mol Cell Biochem* 323:1-7.

Pang PT, Teng HK, Zaitsev E, Woo NT, Sakata K, Zhen S, Teng KK, Yung WH, Hempstead BL, Lu B (2004) Cleavage of proBDNF by tPA/plasmin is essential for long-term hippocampal plasticity. *Science* 306: 487–489.

Pang PT, Lu B (2004) Regulation of late-phase LTP and long-term memory in normal and aging hippocampus: role of secreted proteins tPA and BDNF. *Ageing Res Rev* 3: 407–430.

Parpura V, Chapman ER (2005) Detection of botulinum toxins: Micromechanical and fluorescence-based sensors. *Croat Med J* 46: 491–497.

Patterson SL, Abel T, Deuel TA, Martin KC, Rose JC, Kandel ER (1996) Recombinant BDNF rescues deficits in basal synaptic transmission and hippocampal LTP in BDNF knockout mice.
Neuron 16: 1137–1145.

Pencea V, Bingaman KD, Wiegand SJ, Luskin MB (2001) Infusion of brain-derived neurotrophic factor into the lateral ventricle of the adult rat leads to new neurons in the parenchyma of the striatum, septum, thalamus, and hypothalamus. *J Neurosci* 21:6706-17.

Poo MM (2001) Neurotrophins as synaptic modulators. *Nat Rev Neurosci* 2: 24–32.

Rose CR, R Blum, B Pichler, A Lepier, KW Kafitz, A Konnerth (2003) Truncated TrkB-T1 mediates neurotrophin-evoked calcium signalling in glia cells. *Nature* 426 :74 – 78 .

Rösch H, Schweigreiter R, Bonhoeffer T, Barde YA, Korte M (2005) The neurotrophin receptor p75NTR modulates long-term depression and regulates the expression of AMPA receptor subunits in the hippocampus. *Proc Natl Acad Sci U S A* 102:7362-7.

Rossi C, Angelucci A, Costantin L, Braschi C, Mazzantini M, Babbini F, Fabbri ME, Tessarollo L, Maffei L, Berardi N, Caleo M (2006) Brain-derived neurotrophic factor (BDNF) is required for the enhancement of hippocampal neurogenesis following environmental enrichment. *Eur J Neurosci* 24, 1850-1856.

Rubio N (1997) Mouse astrocytes store and deliver brain-derived neurotrophic factor using the non-catalytic gp95trkB receptor. *Eur J Neurosci* 9 :1847 – 1853.

Saxe MD, Battaglia F, Wang JW, Malleret G, David DJ, Monckton JE, Garcia AD, Sofroniew MV, Kandel ER, Santarelli L, Hen R, Drew MR (2006) Ablation of hippocampal neurogenesis impairs

contextual fear conditioning and synaptic plasticity in the dentate gyrus. *Proc Natl Acad Sci U S A* 103:17501-6.

Sairanen M, Lucas G, Ernfors P, Castren M, Castren E (2005) Brain-derived neurotrophic factor and antidepressant drugs have different but coordinated effects on neuronal turnover, proliferation, and survival in the adult dentate gyrus. *J Neurosci* 25:1089– 1094.

Sahay A, Hen R (2007) Adult hippocampal neurogenesis in depression. *Nat Neurosci* 10:1110–1115.

Scharfman H, Goodman J, Macleod A, Phani S, Antonelli C, Croll S (2005) Increased neurogenesis and the ectopic granule cells after intrahippocampal BDNF infusion in adult rats.. *Exp Neurol* 192: 348-56.

Seri B, García-Verdugo JM, McEwen BS, Alvarez-Buylla A (2001) Astrocytes give rise to new neurons in the adult mammalian hippocampus. *J Neurosci* 21:7153-60.

Schmidt-Hieber C, Jonas P, Bischofberger J. (2004) Enhanced synaptic plasticity in newly generated granule cells of the adult hippocampus. *Nature* 429: 184-187.

Schratt GM, Nigh EA, Chen WG, Hu L, Greenberg M (2004) BDNF regulates the translation of a select group of mRNAs by a mammalian target of rapamycin-phosphatidylinositol 3-kinasedependent pathway during neuronal development. *J Neurosci* 24: 9366–9377.

Shieh PB, Hu SC, Bobb K, Timmusk T, Ghosh A (1998) Identification of a signaling pathway involved in calcium regulation of BDNF expression. *Neuron* 20: 727–740.

Sholl D-A (1953) Dendritic organization in the neurons of the visual and motor cortices of the cat. *J Anat* 87:387–406.

Snyder J-S, Kee N, Wojtowicz J-M (2001) Effects of adult neurogenesis on synaptic plasticity in the rat dentate gyrus. *J Neurophysiol* 85:2423–2431.

Tashiro A, Sandler V-M, Toni N, Zhao C, Gage F-H (2006) NMDA-receptor-mediated, cell-specific integration of new neurons in adult dentate gyrus. *Nature* 442:929–933.

Teng HK, KK Teng, R Lee, S Wright, S Tevar, RD Almeida, P Kermani, R Torkin, ZY Chen, FS Lee, et al (2005) ProBDNF induces neuronal apoptosis via activation of a receptor complex of p75NTR and sortilin. *J Neurosci* 25 :5455 – 5463.

Thoenen H (1995) Neurotrophins and neuronal plasticity. *Science*. 270(5236):593-8.

Thoenen H (2000) Neurotrophins and activity-dependent plasticity. *Prog Brain Res* 128: 183–191.

Thompson NL, BL Steele (2007) Total internal reflection with fluorescence correlation spectroscopy. *Nat Protoc* 2 :878 – 890 .

Tongiorgi E, Righi M, Cattaneo A (1997) Activity-dependent dendritic targeting of BDNF and TrkB mRNAs in hippocampal neurons. *J Neurosci* 17: 9492–9505.

Toni N, Teng EM, Bushong EA, Aimone JB, Zhao C, Consiglio A, van Praag H, Martone ME, Ellisman MH, Gage FH (2007) Synapse formation on neurons born in the adult hippocampus. *Nat Neurosci* 10: 727-734.

Volterra A, Meldolesi J (2005) Astrocytes, from brain glue to communication elements: the revolution continues. *Nat Rev Neurosci* 8:626-40

van Praag H, *et al.* (2002) Functional neurogenesis in the adult hippocampus. *Nature* 415:1030–1034.

von Bartheld CS, Byers MR, Williams R, Bothwell M (1996) Anterograde transport of neurotrophins and axodendritic transfer in the developing visual system. *Nature* 379: 830–833.

von Bartheld CS (2003) Axonal transport and neuronal transcytosis of trophic factors, tracers, and pathogens. *J Neurobiol* 58: 295–314.

Yang J, Siao CJ, Nagappan G, Marinic T, Jing D, McGrath K, Chen ZY, Mark W, Tessarollo L, Lee FS, Lu B, Hempstead BL (2009) Neuronal release of proBDNF. *Nat Neurosci* 12:113-5.

Wang X, Berninger B, Poo MM (1998) Localized synaptic actions of neurotrophin-4. *J Neurosci* 18: 4985–4992.

Wang X, Butowt R, Vasko MR, von Bartheld CS (2002) Mechanisms of the release of anterogradely transported neurotrophin-3 from axon terminals. *J Neurosci* 22: 931–945.

Wigge P, HT McMahon (1998) The amphiphysin family of proteins and their role in endocytosis at the synapse. *Trends Neurosci* 21 : 339 – 344

Zhao C, Teng E-M, Summers R-G, Jr, Ming G-L, Gage F-H (2006) Distinct morphological stages of dentate granule neuron maturation in the adult mouse hippocampus. *J Neurosci* 26:3–11.

Woo NH, Teng HK, Siao CJ, Chiaruttini C, Pang PT, Milner TA, Hempstead BL, Lu B (2005) Activation of p75NTR by proBDNF facilitates hippocampal long-term depression. *Nat Neurosci* 8:1069-77.

Zhao C, Deng W, Gage FH (2008) Mechanisms and functional implications of adult neurogenesis. *Cell* 132: 645-60.

Zigova T, Pencea V, Wiegand SJ, Luskin MB (1998) Intraventricular administration of BDNF increases the number of newly generated neurons in the adult olfactory bulb. *Mol Cell Neurosci* 11: 234-45.

SCIENTIFIC PRODUCTION

Santi S, Cappello S, Riccio M, **Bergami M**, Aicardi G, Schenk U, Matteoli M, Canossa M (2006) Hippocampal neurons recycle BDNF for activity-dependent secretion and LTP maintenance. *EMBO J* 25:4372-80.

Verderio C, Bianco F, Blanchard MP, **Bergami M**, Canossa M, Scarfone E, Matteoli M (2006) Cross talk between vestibular neurons and Schwann cells mediates BDNF release and neuronal regeneration. *Brain Cell Biol* 35:187-201.

Bergami M, Rimondini R, Santi S, Blum R, Götz M, Canossa M (2008) Deletion of TrkB in adult progenitors alters newborn neuron integration into hippocampal circuits and increases anxiety-like behavior. *Proc Natl Acad Sci U S A* 105:15570-5.

Bergami M, Santi S, Formaggio E, Cagnoli C, Verderio C, Blum R, Berninger B, Matteoli M, Canossa M (2008) Uptake and recycling of pro-BDNF for transmitter-induced secretion by cortical astrocytes. *J Cell Biol* 183:213-21.

Bergami M, Berninger B, Canossa M (2009) Conditional deletion of TrkB alters adult hippocampal neurogenesis and anxiety-related behavior. *Communicative & Integrative Biology* 2:14-16.

ACKNOWLEDGEMENTS

I thank Spartaco Santi, Giorgio Aicardi, Magdalena Götz, Roberto Rimondini, Claudia Verderio, Elena Formaggio, Cinzia Cagnoli, Robert Blum, Massimo Riccio, Michela Matteoli, Ursula Schenk, Silvia Cappello, Fabio Bianco, Marie Pierre Blanchard and Eric Scarfone for having collaborated and contributed to the pubblications. R. Jagasia for providing the IRES-DsRed-encoding vector. F.H. Gage for providing the CAG-GFP viral vector. A. Lepier for the retrovirus production. O. Griesbeck for providing the cDNA coding for BDNF-YFP. All members of the Physiological-Genomic department of the LMU in Munich for help during the production of the data, including Ronny, Christophe, Ines and Susi. A very special thank to Marco Canossa and Benedikt Berninger for insightful suggestions and discussions during the design of the experiments, and for providing the necessary scientific environment which significantly contributed to the production of this thesis.